Title: Single-cell characterisation of mononuclear phagocytes in the human intestinal mucosa

Authors: Thomas M. Fenton[1, 2,†*], Line Wulff[1,†], Gareth-Rhys Jones[2], Julien Vandamme[1], Peter B. Jørgensen[1], Calum C. Bain[2], Julie Lee[3], Jose MG. Izarzugaza[4], Kirstine G. Belling[5], Gwo-Tzer Ho[2], Ole H. Nielsen[6], Lene B. Riis[7], Tune H. Pers[8], Henrik L. Jakobsen[9], Allan M. Mowat[10], Søren Brunak[5], William W. Agace[1,11,*]

Affiliations:
[1]Mucosal Immunology group, Department of Health Technology, Technical University of Denmark, Kemitorvet, 2800 Kgs. Lyngby, Denmark
[2]University of Edinburgh Centre for Inflammation Research, Queens Medical Research institute, Edinburgh, EH16 4TJ, UK
[3]Novo Nordisk Foundation Centre for Stem Cell Biology, DanStem, University of Copenhagen, 2200 Copenhagen N, Denmark
[4]Center for Biological Sequence Analysis, Technical University of Denmark, 2800 Lyngby, Denmark
[5]Translational Disease Systems Biology, Novo Nordisk Foundation Centre for Protein Research, Faculty of Health and Medical Sciences, University of Copenhagen, 2200 Copenhagen, Denmark
[6]Department of Gastroenterology, Medical Section, Herlev Hospital, University of Copenhagen, 2730 Herlev, Denmark.
[7]Department of Pathology, Herlev Hospital, University of Copenhagen, 2730 Herlev, Denmark
[8]Novo Nordisk Foundation Centre for Basic Metabolic Research, University of Copenhagen, 2200 Copenhagen N, Denmark
[9]Department of Gastroenterology, Surgical Section, Herlev Hospital, University of Copenhagen, 2730 Herlev, Denmark.
[10]Institute of Infection, Immunity and Inflammation, College of Medicine, Veterinary Medicine and Life Sciences, University of Glasgow, Glasgow, UK
[11]Immunology Section, Lund University, BMC D14, 221-84 Lund, Sweden

[†]These authors contributed equally to this work

[*]Corresponding authors: thomas.m.fenton@gmail.com, wiag@dtu.dk

Abstract

Subsets of mononuclear phagocytes, including macrophages and classical dendritic cells (cDC), are highly heterogeneous in peripheral tissues such as the intestine, with each subset playing distinct roles in immune responses. Understanding this complexity at the cellular level has proven difficult due to the expression of overlapping phenotypic markers and the inability to isolate leukocytes of the mucosal lamina propria (LP) effector site, without contamination by the isolated lymphoid follicles (ILFs), which are embedded in the mucosa and which are responsible for the induction of immunity. Here we exploit our novel method for separating lamina propria from isolated lymphoid follicles to carry out single-cell RNA-seq, CITE-seq and flow cytometry analysis of MNPs in the human small intestinal and colonic LP, without contamination by lymphoid follicles. As well as classical monocytes, non-classical monocytes, mature macrophages, cDC1 and CD103^{+} cDC2, we find that a CD1c^{+} CD103^{-} cDC subset, which shares features of both cDC2 and monocytes, is similar to the cDC3 that have recently been described in human peripheral blood. As well as differing between the steady-state small intestine and colon, the proportions of the different MNP subsets change during different stages of inflammatory bowel disease (IBD) inflammation. Putative cDC precursors (pre-cDC) were also present in the intestine, and trajectory analysis revealed clear developmental relationships between these and subsets of mature cDC, as well as between tissue monocytes and macrophages. By providing novel insights into the heterogeneity and development of intestinal MNP, our findings should help develop targeted approaches for modulating intestinal immune responses.

Introduction

The mononuclear phagocyte (MNP) family consists of classical dendritic cells (cDC), classical monocytes, non-classical monocytes, and macrophages, each of which play specific roles in the induction and function of immune responses, tissue homeostasis and inflammation (Arroyo Portilla et al., 2021; Caër and Wick, 2020; Joeris et al., 2017). Whereas cDC are the main cells involved in the induction and shaping of adaptive immune responses and tolerance (Cabeza-Cabrerizo et al., 2021), macrophages are primarily involved in maintaining tissue homeostasis, and in promoting inflammation in response to infection or tissue damage (Bain and Schridde, 2018; Na et al., 2019). Thus, characterising these populations and understanding their functions under different conditions will be important for improving the treatment of disease and for developing preventative strategies, such as vaccines. However, this has proved difficult due to the expression of overlapping phenotypic markers and due to the heterogeneity within each subset, which is becoming increasingly evident (Brown et al., 2019; Dutertre et al., 2019; Guilliams et al., 2016; Villar and Segura, 2020). This is particularly so in non-lymphoid tissues such as the intestine, where local factors imprint unique adaptations and functions, meaning that each tissue has to be explored independently and at the single-cell level (Blériot et al., 2020).

All MNP subsets are abundant in the human intestine, where they are thought to play important roles in disorders such as the inflammatory bowel diseases ulcerative colitis and Crohn's disease (Bernardo et al., 2018; Viola and Boeckxstaens, 2020). However, much of what is known about intestinal MNPs comes from work in mice and there are very few direct comparisons of these cells in the small and large intestine, which represent anatomical compartments with distinct functions and properties (Mowat and Agace, 2014). Furthermore, although recent work has examined human intestinal leukocytes at the single-cell level (Chapuy et al., 2019; Martin et al., 2019), these studies did not discriminate between cells in the mucosal

lamina propria (LP) and those in the secondary lymphoid organs of the gut-associated lymphoid tissues (GALT), which include the isolated lymphoid follicles (ILFs) which are embedded in the LP (Mörbe et al., 2021; Senda et al., 2019; Spencer et al., 2019). As these compartments have distinct roles in local immunity - with the GALT being responsible for the initiation of antigen-specific B and T cell responses, while the effector responses take place in the LP and epithelium (Barone et al., 2011; Boursier et al., 2005; Masahata et al., 2014) - it is critical to assess their cellular components independently. Recently, we developed a novel technique which allows ILFs of the GALT and the surrounding LP to be isolated separately from human intestinal tissue (Jørgensen et al., 2021). By combining this method with CyTOF, flow cytometry, and IgA-seq, we previously generated an atlas of effector lymphocytes in the LP of the small intestine and colon, and showed that these compartments contain very different populations of T and B cells (Fenton et al., 2020). Here, we have applied the same approaches to analyse the heterogeneity of MNP that are derived unequivocally from the LP of healthy and inflamed human small intestine and colon. As well as separate clusters of mature macrophages, we show that mucosal cDC can be divided into three distinct subsets and, for the first time, describe the presence of putative cDC precursors (pre-cDC) in the human intestine. Trajectory analysis revealed clear developmental relationships between tissue monocytes and macrophages, and between pre-cDC and mature DC. By providing novel insights into the heterogeneity and development of intestinal MNP, our findings should help target approaches for modulating intestinal immune responses.

Results

Single-cell sequencing of MNP subsets from the human intestinal mucosa

To characterise MNP diversity within the human intestinal LP, surgical samples of ileum and colon from uninvolved areas of colorectal cancer patients were processed to remove contaminating GALT and submucosa (SM), as we recently described (Fenton et al., 2020; Jørgensen et al., 2021). Following LP digestion, single-cell RNA sequencing (scRNA-seq) was performed on flow cytometry sorted $CD45^+CD3^-CD19^-HLADR^{int/+}$ cells from ileal and colonic LP cell suspensions, using the 10x Chromium system (**Fig. 1A**). Sequences were obtained from a total of six colonic LP and four paired ileal LP samples (**Table S1**). Distinct clusters of *CD3E*$^+$ T cells, *CD79A*$^+$ B cells, *VWF*$^+$ endothelia, *MS4A2*$^+$ mast cells, *COL3A1*$^+$ stroma, and *NRXN1*$^+$ glia were identified and excluded from further analysis (**Fig. S1A**). Expression of *HLA-DQA1* (MHCII) identified one 'supercluster' and two peripheral clusters (**Fig. S1B**), which were computationally isolated and re-clustered. These 28,758 MHCII$^+$ cells included distinct clusters of *IL3RA*$^+$ pDC, *CLEC9A*$^+$ cDC1, and *FCGR3A*$^+$ non-classical monocytes (**Fig. S1C and 1B**), and a supercluster containing cells expressing either the cDC2-associated marker *CD1C,* the monocyte/macrophage (Mono/Mac) -associated marker *CD14*, or both *CD1C* and *CD14* (**Fig. 1C**). Flow cytometry analysis of colon LP $CD45^+$ $HLA\text{-}DR^+$ $lineage^-$ cells confirmed the presence of CD1c and CD14 single positive cells, as well as a cells expressing variable levels of both CD1c and CD14 (**Fig. 1D**).

To further characterise subsets within this MNP supercluster, these cells were again re-clustered, at high resolution, and were analysed for expression of a curated panel of monocyte, macrophage, and cDC2/3 signature genes (**Fig. 1E**). Three broad populations could be identified, with population 1 (clusters X1-6) expressing the classical monocyte transcription factor *ZBTB16* (Cytlak et al., 2020), population 2 (clusters X7-X20) expressing the macrophage-associated genes *SEPP1, MERTK* and *MAF,* and population 3 (clusters X21-X35) expressing the cDC2/3-

130 associated genes *AP1S3*, *FLT3* and *SEPT6* (Guilliams et al., 2016; Miller et al., 2012), (**Fig. 1E**).
131 The monocyte and macrophage clusters expressed Mono/Mac-specific TFs *ZBTB16*, *MAFB*, and
132 *MAF,* and other TFs involved in tissue-resident macrophage development such as *ID3* (T'Jonck
133 et al., 2018). These were mutually exclusively expressed with the TF *IRF4,* which is associated
134 with cDC2 (Guilliams et al., 2016; Yin et al., 2017) (**Fig. 1E**). Some genes previously used as
135 signature markers to discriminate cDC2/3 from monocytes in blood, such as *FCER1A* and
136 *CLEC10A* (Dutertre et al., 2019), were broadly expressed amongst most clusters, and thus were
137 not useful in segregating these populations in the human gut (**Fig. 1E**).
138
139 As a result of this analysis, all clusters except X36-39 could be identified as putative
140 cDC2/3 or as Mono/Mac (**Fig. 1F**). These remaining clusters expressed both cDC2-associated
141 genes including, *FLT3* and *IRF4,* and Mono/Mac-associated genes, including *CD14* and *C5AR1*
142 (CD88) (**Fig. 1E**). Since cDC3 co-express such markers (Bourdely et al., 2020; Cytlak et al., 2020;
143 Dutertre et al., 2019; See et al., 2017; Villani et al., 2017; Yin et al., 2017) we classified clusters
144 X36-39 as cDC3, of which cluster X38 also expressed a strong IFN-response signature (e.g.
145 *CXCL9*, *CXCL10*, and *WARS*) (**Fig. 1E**).
146
147 To assess the accuracy in designating these clusters as monocytes, macrophages and
148 DC2/3, pseudo-bulk PCA analysis of the clusters was performed using three datasets of MNP
149 gene signatures taken from different studies using blood cDC2, classical monocytes, and *in vitro*
150 monocyte-derived macrophages (Carpentier et al., 2016; Goudot et al., 2017) which were
151 previously collated (Tang-Huau et al., 2018). Consistent with our first supervised analytical
152 approach, these clusters again separated into three groups, with PC1 driving separation of
153 cDC2/3 and PC2 separating monocytes from macrophages (**Fig. 1G**). In summary, while showing
154 a high degree of transcriptional overlap, by combining high resolution clustering and gene

155 expression analysis of published data sets we were able to separate intestinal LP MNP into
156 monocytes, macrophages, cDC1, pDC and cDC2/3.
157
158 **Human intestinal CD1c$^+$ MNP include both cDC2 and cDC3**
159 To further explore diversity within the cDC2/3 populations, clusters X21-39 (Fig. 1F) were
160 computationally isolated and re-clustered, and six distinct clusters were identified (**Fig. 2A**).
161 Clusters Y5 and Y6 expressed Mono/Mac-associated genes, including *S100A9*, *CD163, FCN1*
162 and *FCGRT,* and showed lower expression of *IRF4* compared with the other clusters, indicative
163 of cDC3 (Bourdely et al., 2020; Girard et al., 2020) (**Fig. 2B and C**). In contrast, cluster Y2 lacked
164 expression of Mono/Mac-associated genes, and expressed genes previously associated with
165 cDC2, including *CD207*(Lim et al., 2020; De Monte et al., 2016)*, NET1*(Girard et al., 2020)*,* and
166 *IRF4*(Dutertre et al., 2019)(**Fig. 2B and C**). Y2 also highly expressed other signature genes
167 enriched in human blood cDC2 vs cDC3 (Bourdely et al., 2020), including *ZEB1*, *ADAM19* and
168 *LAD1* (**Fig S2A**). Interestingly, cluster Y5 contained the CXCL9$^+$ CXCL10$^+$ cells identified in Fig.
169 1 as potentially responding to IFN (**Fig. 2D and S2B**). Thus, cluster Y2 appeared to contain bona
170 fide cDC2, while Y5 and Y6 contained cells resembling cDC3. In order to investigate possible
171 functional differences between the cDC2 and cDC3, we assessed their differential expression of
172 immunologically relevant genes which could have been missed by statistical tests of differential
173 expression. cDC2 and cDC3 showed differential expression of multiple genes with immune
174 functions, including Fc receptors and cytokines, as well as transcription factors, suggesting
175 possible functional differences between the cells (**Fig. 2D**).
176
177 Cluster Y3 showed mixed expression of cDC2 and cDC3 signatures (**Fig. 2C, Fig S2A**), but
178 expressed genes associated with stimulus-response, including *FOS* and *JUN* (**Fig. 2B and S2C**).
179 This cluster contains a heterogeneous mix of cDC2 and cDC3 cells which were clustered together

180 due to shared transcriptional states rather than lineage identities. Finally, Clusters Y1 and Y4
181 expressed low levels of MHCII genes and high levels of cell-cycle associated genes, including
182 *KIAA0101* and *MKI67* (**Fig. 2C and S2C**), and thus resembled precursors and will be further
183 discussed below.
184
185 **Human CD1c^{+}CD14^{low} intestinal cDC3 can be distinguished from cDC2 by low levels of**
186 **CD103 and CD207**
187 To identify surface markers that have the potential to distinguish intestinal cDC2 from cDC3, a
188 Legendscreen antibody panel was used to screen for surface antigens which showed a bimodal
189 expression pattern on colonic CD1c^{+}CD14^{low} MNP. Of 288 surface markers, only CD1a, CD11a,
190 CD103, CD206, and CD207 showed bimodal expression within CD1c^{+}CD14^{-} MNP (**Fig. S2D**). To
191 map expression of these surface markers to the cDC2/3 scRNA-seq clusters, these antibodies
192 were included within a CITE-seq panel to stain intestinal LP cell suspensions (3 colon LP samples
193 and 1 matched ileal LP sample). The main cDC2 cluster, Y2, expressed moderate-to-high levels
194 of CD103, high levels of CD207, and relatively low levels of CD11a (**Fig. 2E**). In contrast, the
195 cDC3 clusters Y5 and Y6 expressed low levels of CD103 and CD207, but both clusters uniformly
196 expressed CD11a at high levels (**Fig. 2E**). CD14 and CD209 were expressed at only low levels
197 in all clusters, but both showed highest expression within the cDC3 cluster Y5 (**Fig. S2D**). Finally,
198 CD5, which has been used as a specific surface marker of human blood cDC2 vs. cDC3(Bourdely
199 et al., 2020; Cytlak et al., 2020; Dutertre et al., 2019; Yin et al., 2017), was expressed by only a
200 small fraction of cells in both intestinal cDC2 cluster Y2 and cDC3 cluster Y6 (**Fig. S2E**). To define
201 intestinal cDC2 vs cDC3 using surface markers, the co-expression of CD103, CD207 and CD11a
202 was analysed using CITE-seq, and cDC2 were defined as CD103^{+} and/or CD207^{+} CD11a$^{-/low}$
203 cells, while cDC3 were defined as CD103^{-} CD207$^{low/-}$ CD11a^{hi} cells (**Fig. 2F**). Clusters Y3 and Y4
204 both showed a mix of CD103^{+} CD207^{+} CD11a^{-} and CD103^{-} CD207^{-} CD11a^{+} expression (**Fig.**

S2F). Thus, putative cDC3 can be distinguished from cDC2 in the human intestinal LP by high expression of CD11a, low expression of CD103, and moderate-to-low expression of CD207.

The human intestinal LP contains precursors of cDC1, cDC2 and cDC3

Conventional DC are derived from pre-cDC, and recent studies have identified committed precursors of cDC1 (pre-cDC1), cDC2 (pre-cDC2), and, more recently, cDC3 (pre-cDC3) (Bourdely et al., 2020), as well as uncommitted pre-cDC precursors in human peripheral bone marrow, blood (Breton et al., 2015; Cytlak et al., 2020; See et al., 2017; Villani et al., 2017), and tonsils (Durand et al., 2019). Given that some intestinal cDC clusters in this dataset shared characteristics with cDC precursors (Fig. 2) - and to explore the relationships between these cells and mature cDC subsets - the cDC1, cDC2, and cDC3 clusters were computationally isolated and re-clustered together, and tSpace (Dermadi et al., 2020) was used to perform trajectory analysis. The tSpace principle components were used for a trajectory-based clustering and visualisation by 2D representation of 3-dimensional tSpace UMAP (Flat tUMAP). Cells of the previous cDC2 (Y2) and cDC3 (Y5/6) clusters again grouped together in this clustering, while cDC1 were separate, but all subsets extended individual branches to meet at the connection between Y1, Y4, and cDC1 (**Fig. 3A**). The clusters at the tips of these branches expressed a proliferation signature, defined by high expression of the cell-cycle-associated genes, including *STMN1*, *KIAA0101*, and *MKI67*, which is characteristic of pre-cDC (**Fig. 3B**) (Balan et al., 2018; Brown et al., 2019; Chen et al., 2016; Durand et al., 2019; Ma et al., 2019). By re-clustering all cDC at high resolution, 42 new cDC clusters were identified (**Fig S3A**), and to focus on putative cDC precursors, all clusters outside of the proliferating branches were grouped into putative mature cDC1, cDC2, and cDC3 clusters (**Fig. 3C**), and these identities were confirmed by expression of the signature genes *CLEC9A*, *IRF4*, and *C1QA* (**Fig. 3D**). The remaining clusters D1, D3, D4, and D7-D9 all expressed a proliferation signature, while clusters D1, D3, D4 and D7 all expressed

low levels of MHCII genes (**Fig. 3E**), which has been described for mouse and human pre-cDC (Cabeza-Cabrerizo et al., 2021; Villani et al., 2017). Clusters D3, D4 and D7 also expressed low levels of the CD11c gene *ITGAX*, compared with mature cDC2/3 (**Fig. 3E**), which is characteristic of early cDC precursors (Cytlak et al., 2020). Clusters D3 and D7 expressed high levels of the pDC-associated genes *LILRA4* and *GZMB* (**Fig. 3E**), which suggests that these may be the most developmentally close to early pre-cDC (See et al., 2017). Finally, clusters D1, D3, D7 and D8 expressed the highest relative 'stemness' score, composed of 20 genes expressed in our dataset (*BUB1, CCND2, CDC6, CDT1, CKS2, COL18A1, CSRP2, DTYMK, HELLS, KPNA2, MCM2, MCM4, MCM5, NAP1L1, PCNA, RRM2, SHROOM3, SMO, TOP2A, TTK*) out of 40 genes which were previously identified as forming a general 'stemness' signature (Koeva et al., 2011) (**Fig. S3B**). Thus, clusters D1, D3, D4, D7 and D8 are a heterogeneous mix of proliferating cells, each showing multiple features of pre-cDC. Clusters D9 and D10 expressed *CCR7*, *CD80* (B7-1), *LAMP3* (DC-LAMP), and *CD80*, as well as *CD207* and *C1QA* (**Fig. 3E**), were therefore identified as mixed clusters of migratory cDC2/3.

Heterogeneity of human intestinal LP pre-cDC

The pre-cDC cluster D1 expressed the cDC1-associated genes *IRF8*, *BATF3, CADM1, ID2* and *CLEC9A*, as well as moderate levels of *XCR1* (**Fig. 3D and E**). Cluster D1 connected to D2 then to mature cDC1 in the tUMAP embedding, with the former expressing higher levels of *RUNX3*, *THBD*, and the pre-cDC-associated *CLEC4C* (See et al., 2017) (**Fig. 3E**). In contrast, cluster D2 and the mature cDC1 expressed higher levels of *XCR1* and *CADM1* than cluster D1 (**Fig. 3E**). In agreement with the mouse literature (Grajales-Reyes et al., 2015), *NR4A1* and *ATF3* were upregulated during the transition from D2 to the mature cDC1 cluster (**Fig. 3C**). Collectively, these results suggest that cluster D1 and D2 may represent early and late pre-cDC1, respectively.

The pre-cDC clusters D3 and D4 expressed genes associated with the cDC2 lineage, including *IRF4*, *CD1C* and *IL-22RA2*; transcription factors associated with haematopoiesis, including *PRDM16* (Tang-Huau et al., 2018), *KIT* (Thorén et al., 2008), *SOX4* (Ma et al., 2019) and *CXXC5* (Joshi et al., 2020); *S100B* and *LTB,* which are expressed on proliferating pre-cDC in the human tonsil (Durand et al., 2019); and *NGFR* and *CDH1*, the proteins of which have been previously identified as cell surface markers of pre-cDC (Dutertre et al., 2019) (**Fig. 3E**). Cluster D4 did not express cell-cycle genes to the same extent as D3, but expressed the highest level of the haematopoiesis genes, and the highest level of the pDC-associated genes *LILRA4* and *GZMB* (**Fig. 3E**). D4 also expressed low levels of *CD1C*, which aligns with previous data on early pre-cDC subsets (See et al., 2017) (**Fig. 3E**). Thus, clusters D3 and D4 appear to be distinct subsets of pre-cDC2, with D4 perhaps representing an earlier precursor.

Proliferating clusters D7, D8 and D9, which were connected in the tUMAP embedding to mature cDC3 (**Fig. 3C**), all expressed cDC3 markers such as *C1QA*, *CD14*, and *CD163* (**Fig. 3D and E**). These cells also expressed higher levels of several genes associated with pre-DC in blood, including *AXL* and *IL3RA* (Brown et al., 2019; Cytlak et al., 2020; See et al., 2017; Villani et al., 2017) although these are also expressed by the mature cDC3 (**Fig 3E**). Of these three clusters, D7 expressed the highest level of the cell-cycle genes and the myelopoiesis-associated gene *CD38*, and the lowest level of MHCII genes (**Fig. 3E**). Collectively, these results suggest that clusters D7-D9 represent a heterogeneous mix of pre-cDC3, with D7 perhaps representing the earliest precursor.

To assess the direction in which the putative pre-cDC clusters might be related, RNA velocity of the clusters was analysed and overlayed on the tUMAP embedding**.** Analysis of RNA splicing patterns demonstrated a clear directionality between pre-cDC1 clusters D2 and D3, with a less

pronounced velocity to mature cDC1 cluster D4 (**Fig. 3F)**. There was clear directionality from pre-cDC2 cluster D4 to mature pre-cDC2 and from pre-cDC3 cluster D7 to mature cDC3 (**Fig. 3F)**. Directionality was unclear between the pre-cDC clusters D1, D3, D4 and D7, with D3 or D4 seemingly upstream of D1 and D7 (**Fig. 3F)**. The data showed similar results when ileal and colonic samples were analysed separately (**Fig. S3C**). To further analyse cluster relationships, the pseudotime of each cluster was analysed using the most proliferative cluster, D7, as the starting point for pseudotime calculation The putative lineage-specific precursors (D1, D3/4, and D7) each had low pseudotime scores compared with their mature counterparts, supporting their identities as precursors, while the putative migratory clusters (D5 and D6) had the highest pseudotime scores, supporting their identities as highly mature cDC (**Fig. 3G**).

Characterising intestinal LP monocyte and macrophage populations

Murine intestinal monocytes develop into macrophages along a 'waterfall' of phenotypic intermediates which is interrupted during inflammation, leading to the preferential accumulation of pro-inflammatory cells at the expense of mature macrophages (Bain et al., 2013, 2014; Desalegn and Pabst, 2019; Rivollier et al., 2012). To investigate whether a similar monocyte 'waterfall' exists in the human intestine LP, ileal and colonic LP cells identified as Mono/Mac in Fig. 1 were isolated and trajectory analysis was performed with tSpace (Dermadi et al., 2020). The tSpace principal components were used for trajectory-based reclustering and tUMAP embedding, which resulted in 11 Mono /Mac clusters (M1-M11) (**Fig. 4A**). DEG analysis of the trajectory-based clusters identified high levels of monocyte-associated genes, such as *S100A9*, *FCN1* and *VCAN* (Bujko et al., 2018; Villani et al., 2017), in cluster M1 (**Fig. 4B and C**). To

investigate the downstream developmental trajectories, pseudotime scoring was performed on the tSpace trajectories using the M1 monocyte cluster as the pseudotime starting point, and averaging all trajectories from there. This demonstrated a pseudotime trajectory from cluster M1, via M2-M3, then M4-M6, and ending at M7-M10 (**Fig. 4D**). Cluster M11 was considered too small to analyse pseudotime with confidence.

To investigate heterogeneity of the monocyte-derived clusters, DEG analysis showed clusters M2 and M3 as expressing intermediate levels of *S100A9*, *VCAN*, and *ITGAX* and low levels of *C1QC*, which we classified as early intermediate cells; clusters M4-6, which lacked expression of *S100A9* and *FCN1* and expressed intermediate levels of *ITGAX* and *C1QC*, which we classified as late intermediate cells; and cluster M7 and M8 that expressed high levels of *CD209* and *C1QC*, which is consistent with mature macrophages (Bujko et al., 2018; Schridde et al., 2017) (**Fig. 4B and C**). The two small clusters M9 and M10 shared some features with mature macrophages, including high expression of MHCII and C1Q genes, but expressed low levels of *CD209* and *CD163* (**Fig. 4B and C**). Finally, the smallest cluster, M11, expressed very high levels of cell-cycle associated genes including *MKI67* and *KIAA0101*, indicating that these represented a population of proliferating cells (**Fig. 4B and C**).

In recent single-cell data, murine monocytes were found to develop into resident macrophages along two distinct paths, defined by the expression or absence of pro-inflammatory pathways (Desalegn and Pabst, 2019). To investigate this possibility in human intestinal Mono/Mac, signalling pathway activity was analysed using the Pathway RespOnsive GENes (PROGENy) package, which infers pathway activity within cells using expression levels of pathway response genes (Schubert et al., 2018) (**Fig. 4E**). PROGENy analysis showed activation of NFκB and TNFα signalling pathways in the monocyte cluster M1 and in the early intermediate cluster M3, but not

in the parallel early intermediate cluster M2 (**Fig. 4E**). Consistent with this, cluster M3 expressed high levels of pro-inflammatory cytokines including *IL1B, CXCL8* (IL8), and *CCL4* (MIP-1β), as well as the signalling protein *NFKBIA* (**Fig. 4B** and F). This dichotomy extended to late intermediate as well as mature macrophage clusters, with the late intermediate cluster M5 and the mature macrophage cluster M7 showing indications of enhanced NFκB and TNF signalling, and enhanced expression of higher pro-inflammatory cytokines, compared with other late intermediate and mature macrophage clusters (**Fig. 4B and F**). Clusters M3, M5 and M7 also showed higher activation of MAPK and EGFR pathways (**Fig. 4E**). In contrast, the late intermediate clusters M4 and M6, and the mature macrophage clusters M8 and M9, all showed evidence of increased activation of the JAK-STAT and WNT signalling pathways (**Fig. 4E**). Interestingly, three of the 4 mature macrophage clusters (M7-M9) showed evidence of responding to TGFβ signalling (**Fig. 4E**), consistent with previous work in mice (Schridde et al., 2017). These clusters also showed evidence of p53 pathway activation, which is involved in multiple aspects of cell function including cell-cycle arrest, and which was not active in the proliferating cluster M11 (**Fig. 4E**). In contrast, M11 showed evidence of responding to oestrogen (**Fig. 4E**), consistent with findings that oestrogen may drive macrophage proliferation (Pepe et al., 2018).

As well as showing a putative pro-inflammatory phenotype, clusters M5 and M7 expressed the stimulus-response genes *FOS, JUN,* and *EGR1* (Bahrami and Drabløs, 2016) (**Fig. 4B and G**), and other transcription factors including *KLF2, KLF4* and *KLF6* (**Fig. 4B**). The Discriminant Regulon Expression Analysis (DoRothEA) package, which infers transcription factor activity from expression of downstream target genes, was used to further investigate this heterogeneity in transcription factor activity (Garcia-Alonso et al., 2019; Holland et al., 2020). This supported activity of transcription factors including Nuclear Factor kappa-light-chain-enhancer of activated

B cells (NFκB) and Activator Protein-1 (AP-1) in clusters M1, M3, M5, and M7, and additionally identified activity of Activating Transcription Factor (ATF) in clusters M5 and M7 (**Fig. S4A**). In contrast, clusters M4, M6, M8 and M9 showed inferred activity of the transcriptional repressor RE1-Silencing Transcription factor (REST), and the MHCII promoter-associated regulatory factor X5 (RFX5) (**Fig. S4A**). Interestingly, cluster M6 also expressed the stimulus-response genes and KLF genes (**Fig. 4B and G**), but this cluster showed activation of the JAK-STAT and WNT pathways instead of the NFκB, TNFα MAPK, and EGFR pathways (**Fig. 4E**), it expressed low levels of pro-inflammatory cytokines (**Fig. 4F**), and showed particularly low activation of *JUN* and *FOS* (**Fig. S4A**). Thus, clusters M3, M5, and M7 seem to share a stimulus-response and pro-inflammatory profile, while clusters M2, M4, and M6 seemed to share a less-inflammatory profile.

Clusters M5, M6, M7, and M10 also expressed the transcription factor *KLF2*, which has been implicated in efferocytosis, and clusters M6 and M7 expressed the efferocytosis-associated gene *STAB1*, suggesting they may be specialised for uptake of apoptotic cells (**Fig. 4H**)(Elliott et al., 2017). Two other efferocytosis-associated genes, *AXL* and *MERTK*, were expressed by clusters M4-M9 and M7-M9, respectively (**Fig. 4H**). Thus, the late intermediate clusters M4-M6 and mature macrophages M7-M9 seem to be involved in efferocytosis, but, in line with a recent study (Lantz et al., 2020), there is heterogeneity in the expression of genes involved.

To understand how the intestinal macrophage subsets (M7-10) may be related to previously describe tissue resident macrophage subsets, we further explored genes differentially expressed by these subsets. The macrophage clusters M7, and, to a lesser extent, M8, were both enriched in gene signatures of perivascular macrophages (Silva et al., 2021), including *LYVE1, SIGLEC1* (CD169)*, FOLR2,* and *MAF* (**Fig. 4B and I**), consistent with the finding that the majority of mature macrophages in the LP are found in a perivascular niche (Honda et al.,

2020). CD169^{+} macrophages have also been observed in mouse intestines (Hiemstra et al., 2014), where they seem to play a role in surveillance of the vasculature (Kang et al., 2020).

The small *CD163*^{lo} mature macrophage cluster, M9, expressed relatively high levels of *CD4, C2*, and *ADAMDEC1* (**Fig. 4B and J**), and in this respect resembled non-monocyte-derived self-maintaining resident macrophages, as previously described in the murine intestine (De Schepper et al., 2018; Shaw et al., 2018). These cells also highly expressed matrix metalloproteinases, including *MMP9* and *MMP12* (**Fig. 4B and J**), which was also reported for self-maintaining murine intestinal macrophages (De Schepper et al., 2018), and these cells might therefore be involved in tissue remodelling or angiogenesis. The other *CD163*^{lo} macrophages, in cluster M10, expressed genes associated with iron sequestration (*FTL*), vitamin A metabolism (*RBP1*), microglia (*PLP1*, *PMEPA1,GPM6B*) and fibrosis (*SPARC*), as well as the adipocyte-associated genes *ADIRF* and *SCD* (**Fig. 4B**), and showed poor activation of most of the response pathways (**Fig. 4E**) and transcription factor activity (**Fig. S4A**), so did not have a clear phenotype. They did however resemble adipose tissue macrophages in several respects(Frey and Vogel, 2011; Li et al., 2020), including activity of the TRAIL pathway (**Fig. 4E**) (Maixner et al., 2020).

In summary, ileal and colonic LP Mono/Mac are highly heterogeneous, encompassing a differentiation spectrum from monocytes (M1) through early (M2, M3) and late (M4, M5, M6) intermediate cells, to mature macrophages (M7, M8), as well as small populations resembling self-maintaining macrophages (M9), adipose tissue-like macrophages (M10), and proliferating cells without a clear identity (M11). Monocytes appear to develop into macrophages via both a pro-inflammatory route (M1- M3- M5- M7) and a parallel less-inflammatory route (M1- M2- M4- M6- M8).

405

406 **Analysis of Mono/Mac subsets by surface marker expression**

407 To identify surface antigens that could be used to distinguish the different stages of intestinal
408 monocyte development by flow cytometry, colonic CD14^{+}CD1c^{lo} cells were screened for surface
409 antigens which showed heterogeneous expression, using the Legendscreen. Of 288 antibodies
410 tested, colonic CD14^{+}CD1c^{lo} cells expressed heterogenous levels of CD11a (LFA1/*ITGAL*),
411 CD11b (*ITGAM*), CD11c (*ITGAX*), CD13 (*ANPEP*), CD18 (*ITGB2*), CD39 (*ENTPD1*), CD50
412 (*ICAM3*), CD55 (DAF), CD81, CD89 (FCAR), CD90, CD163, CD206 (mannose receptor/*MRC1*),
413 CD274 (PDL1), CD276, and CD301 (CLEC10A) (**Fig. S4B**), indicating that these could be used
414 as surface markers to distinguish distinct subsets. Of these CD11c, CD11a, CD206, and CD55
415 together with CD14 and CD1c were selected to use in a CITE-seq panel to determine their levels
416 of expression on clusters M1-M11 (**Fig. 4K**). CD55 was highly expressed by the monocyte cluster
417 M1, expressed at intermediate levels on early intermediate clusters M2 and M3, and was not
418 expressed on late intermediate clusters M4 and M5, or mature Mac (**Fig. 4K**). CD11a was highly
419 expressed on monocyte (M1) and early intermediate clusters (M2 and M3), and was expressed
420 at intermediate levels on late intermediate clusters (M4 and M5) (**Fig. 4K**). In contrast, CD206
421 was induced at the late intermediate stage of development and was maintained on mature
422 macrophage clusters, but was not present on the small M9 and M10 clusters (**Fig. 4K**). CD1c was
423 poorly expressed by monocytes and macrophages, but was expressed at moderate levels on all
424 intermediate clusters (M2-M6). This aligned with the observed expression of cDC2-associated
425 genes *CD1C*, *CD1E*, *CLEC10A*, and *FCER1A* in monocyte-derived intermediate clusters (**Fig.**
426 **4B**). CD11c was expressed at moderate levels on monocytes and increased during development
427 of intermediate clusters M2-M6, then it was expressed at moderate-to-high levels on clusters M8
428 and M9 and low levels on M7 and M10 (**Fig. 4K**). Cluster M7 was distinguished from other mature
429 macrophages by particularly high CD14 expression, while M9 and M10 could be identified as

uniquely CD206^{-} CD11c^{+} and CD206^{-} CD11c^{-} macrophages, respectively (**Fig. 4K**). In summary, a panel of surface markers was used to identify heterogeneity and likely developmental stage within intestinal monocytes and macrophages.

Site-specific differences in MNP subsets

Given the non-redundant role individual MNP subsets play in intestinal homeostasis and disease, we used our scRNA-seq and CITE-seq analyses to design an antibody panel that would allow assessment of potential regional and inflammation-associated alterations in intestinal MNP subset composition by flow cytometry. To maximise the number of MNP subsets which could be analysed in small biopsy samples, we designed an antibody panel which would identify multiple MNP subsets by flow cytometry, in a single tube. Among the viable CD45^{+} CD3^{-} CD19^{-} HLA-DR$^{int/+}$ cells, cDC2 were identified as CD14^{-} CD141^{-} CD1c^{+} CD11a^{-} CD103^{+} cells, while cDC3 were identified as CD14^{-} CD141^{-} CD1c^{+} CD11a^{+} CD103^{-} cells (**Fig. 5A**). Using this panel, we additionally found that cDC2 exclusively expressed CD1a, while cDC3 exclusively expressed CLEC12A (**Fig. 5B**). When assessing subset frequencies in 10 matched ileal and colonic samples, cDC2 dominated the CD1c^{+} DC population of the ileum, but cDC2 and cDC3 were present at equivalent frequencies in the colon (**Fig. 5C**). Thus, human intestinal CD1c^{+} cells can be separated by flow cytometry into CD1c^{+} CD103^{+} CD1a^{+} cDC2 and CD1c^{+} CD11a^{hi} CLEC12A^{+} putative cDC3.

To identify the different Mono/Mac subsets, CD14$^{int/+}$ cells were divided into two fractions consisting of CD55^{+} CD206^{-} and CD55^{-} CD206$^{+/-}$ cells (**Fig. 5D**). The CD55^{+} CD206^{-} cells contained HLA-DR^{int} monocytes and HLA-DR^{+} early intermediate cells. The CD55^{-} CD206$^{+/-}$ fraction was first divided into CD11a^{+} CD163^{-} late intermediate and CD11a^{-} CD163$^{int/+}$ mature macrophages (**Fig. 5D**). Finally, the macrophages were divided into CD163^{int} CD14^{int} and CD163^{hi}

455 CD14^{hi} macrophages. Although CD14 and CD163 showed a continuous spectrum of expression,
456 there was a clear division between intestinal sites, with significantly more CD163^{int} CD14^{int}
457 macrophages in the ileum than in the colon (**Fig. 5E**). The CD206^{-} macrophage populations
458 (related to scRNA-seq clusters M9 and M10) were too small to identify with confidence in
459 individual patient samples. However, after concatenation of 10 matched ileal and colonic LP
460 samples, CD55^{-} CD11a^{-} CD206^{-} CD14^{int} CD163^{int} cells could be identified as 0.61% of ileal and
461 1.71% of colonic LP macrophages, respectively (**Fig. S5C**).
462
463 **Inflammation-associated changes to MNP subset frequencies**
464 To assess the impact of intestinal inflammation on the relative abundance of MNP subsets in the
465 intestinal LP, we analysed biopsies taken during routine endoscopic procedures for initial disease
466 assessment or disease surveillance. Biopsies were taken from multiple sites per patient, and the
467 extent of inflammation at each site was classified using standard IBD scoring (see Methods) as
468 either quiescent, mild, or moderate. In these biopsies, there was a positive correlation of cDC3
469 and a negative correlation of cDC2 with the severity of colonic inflammation (**Fig. 5F**), and a
470 similar trend was found in the ileum (**Fig. S5D**). Analysis of cDC2 and cDC3 as a proportion of
471 total CD45^{+} lineage^{-} HLA-DR^{+} MNP showed that this was due to a reduction in cDC2 compared
472 with total MNP, rather than a relative expansion of cDC3 (**Fig. S5E**).
473
474 Some of the IBD patients recruited were undergoing anti-α4β7 antibody (Vedolizumab) therapy,
475 and in these patients we noticed a dramatic reduction of total CD1c^{+} MNPs in biopsy samples
476 (**Fig. 5G and H**). We found that patients treated with Vedolizumab had lower frequencies of both
477 CD1c^{+} CD103^{+} cDC2 and CD1c^{+} CD103^{-} cDC3 in the intestinal LP (**Fig. 5I**), while they retained
478 CD14^{+} cells (Mono/Mac) (**Fig. S5F**). The loss of both cDC2 and cDC3 after Vedolizumab

treatment, while monocytes and macrophages were retained, supports the definition of human intestinal CD1c^{+} CD103^{-} MNP as a conventional DC subset, and not as monocyte-derived cells.

Finally, we also analysed Mono/Mac subset frequencies in digested biopsies taken from IBD patients using flow cytometry. Because cell numbers were lower in biopsies than in resection samples, CD55^{+} CD206^{-} HLA-DR^{int} monocytes could not be reliably distinguished from CD55^{+} CD206^{-} HLA-DR^{+} early intermediate cells, so both were collected together in the CD55^{+} CD206^{-} gate. We found that increased severity of endoscopic inflammation was associated with an increase in both combined monocyte/early intermediate and in late intermediate cells in the colon (**Fig. 5J**) and ileum (**Fig. S5G**). The frequency of late intermediate cells was slightly increased in quiescent IBD samples compared with non-IBD controls, and was equivalent between mild and moderate IBD inflammation. However, the frequency of combined monocyte/early intermediate cells was only increased when inflammation was present (**Fig. 5J and S5G**). Human intestinal monocyte-derived cells therefore act similar to those of the mouse in inflammation, with an increase of monocyte and intermediate cells, and a reduction of mature macrophages.

Discussion

MNPs play critical roles in tolerance, immunity and inflammation at the intestinal barrier and characterizing the individual members of this family will be crucial for understanding immune responses in the gut during health and disease. Here, we used scRNA-seq to characterise MNPs of the human intestinal LP, which is the largest site of immune surveillance in the gut. Much research focus of the last decade has been spent on deciphering MNP subset identities in mice and humans, an undertaking that has been complicated by their overlapping phenotypes (Bogunovic et al., 2009; Cytlak et al., 2020; Dutertre et al., 2019; Guilliams et al., 2016; Satpathy et al., 2012; Schlitzer et al., 2015; Tamoutounour et al., 2012; Varol et al., 2009; Villani et al., 2017). Human MNPs are classically defined by their expression of HLA-DR and lack of specific lineage markers such as CD3 and CD19, and are usually further divided into $CD14^+$ Mono/Macs and $CD14^-$ cDC (Caër and Wick, 2020). Here we used a relatively non-stringent gating strategy to enrich cells by FACS sorting before sequencing, to ensure comprehensive capture of all MNP subsets, including any $MHCII^{lo}$ cells such as pre-cDC and monocytes.

Together with clearly separate clusters of pDC and cDC1, a small population of $FCGR3A^+$ non-classical monocytes was also found on initial analysis, but whether these were in the intestinal parenchyma itself is unclear. Non-classical monocytes are generally thought to function as MNP patrolling the vasculature (Carlin et al., 2013) and we identified substantial numbers of vascular and lymphatic endothelial cells in our preparations. Although this suggests that at least some of the non-classical monocytes we found may have been within the vasculature, there is some evidence that non-classical monocytes can migrate into tissues including the intestine (Schleier et al., 2020). Thus, the exact location of these non-classical monocytes remains an open question. Unlike the cDC1, pDC and non-classical monocytes, the cDC2, cDC3, classical monocytes, and macrophages all showed a high degree of transcriptional overlap, and high resolution analysis

was required to reveal distinct clusters of these cells. At least part of this transcriptional overlap involved shared expression of stimulus-response-associated genes, including *FOS*, *JUN*, and *EGR1*, and antigen presentation genes, including MHCII and CD1 genes. Similarly, although we attempted to regress out the effect of cell-cycle-associated genes, these continued to represent confounding issues when attempting to separate cDC2, cDC3, and Mono/Mac into discrete clusters. To circumvent the effect of these dominant shared state-specific genes, we used high resolution clustering and an iterative process involving both biased and unbiased approaches, to define cell identities.

Using this strategy, we were able to discriminate defined populations expressing signature genes of classical monocytes, macrophages and cDC2, but we also found a group of cells which expressed both monocyte- and cDC2-associated genes. Human MNPs with these characteristics have historically been identified as monocyte-derived DC ("moDC") (Tang-Huau and Segura, 2019) and DC-like cells can be derived from human monocytes *in vitro* (Sallusto and Lanzavecchia, 1994). However, recent scRNA-seq analyses have revealed a unique cell with monocyte- and cDC2-associated characteristics, named cDC3 (Bourdely et al., 2020; Cytlak et al., 2020; Dutertre et al., 2019; Villani et al., 2017). By extending our scRNA-seq findings with flow cytometry and CITE-seq, we confirmed previous reports that two subsets of $CD1c^+$ intestinal cDC2-like cells could be defined based on their expression of CD103 (Bernardo et al., 2016; Jaensson et al., 2008; Mann et al., 2015; Watchmaker et al., 2014). In our hands, these separated into a population of $CD103^+$ $CD1a^+$ cells that were consistent with *bona fide* cDC2, and a population of $CD103^-$ $CD11a^+$ $CLEC12A^+$ cells which had the characteristics of cDC3. These cDC3 not only expressed a number of monocyte-associated genes and were enriched in the colon compared with the ileum, but also expanded relative to cDC2 during active IBD inflammation. This could perhaps be explained by their expression of higher levels of *SELL* (coding for L-selectin),

551 an adhesion molecule which has been associated with myeloid cell migration to the inflamed
552 intestine (Habtezion et al., 2016).
553
554 It should be noted that although the cDC3 we identified expressed monocyte-associated genes,
555 it seems unlikely that they are derived from monocytes, as their numbers were significantly
556 reduced in IBD patients that had been treated with anti-integrin α4β7 antibody (Vedolizumab)
557 therapy, an intervention which we and others have shown does not affect monocyte proportions
558 in the LP (Schleier et al., 2020). In contrast, α4β7 has been shown to play a role in the homing
559 of cDC to the murine intestine (Villablanca et al., 2014) and our Vedolizumab-treated patients
560 showed reduced proportions of cDC2. These findings have potential implications for the use of
561 anti-integrin α4β7 as a long-term IBD therapeutic, as although blocking the migration of pro-
562 inflammatory cDC activity into the gut could be beneficial, cDC are also crucial for the induction
563 of tolerance to the microbiota in the gut (Ohnmacht et al., 2009; Travis et al., 2007; Worbs et al.,
564 2006).
565
566 Although it remains possible that $CD1c^+$ $CD103^+$ and $CD1c^+$ $CD103^-$ MNP in the intestine merely
567 represent different states of cDC2, cDC3 in humans have recently been described as forming a
568 distinct lineage from cDC2 (Cytlak et al., 2020). In support of this possibility, we identified distinct
569 populations of potential cDC precursors in the LP, including pre-cDC1, pre-cDC2, and pre-cDC3.
570 These clusters showed low expression of MHCII genes, high expression of cell-cycle-associated
571 genes and mixed expression of other hematopoietic and pre-cDC-associated genes. As well as
572 the $MHCII^{lo}$ clusters, there were other proliferating, closely related clusters which also expressed
573 cell-cycle genes to different extents, which could be developmentally intermediate or immature
574 cDC. Recent work has suggested that cDC3 develop along a distinct developmental trajectory
575 from cDC1 and cDC2 (Cytlak et al., 2020), but here, the developmental relationships between the

576 proliferating cDC/pre-cDC clusters was not clear. These findings suggest that a variety of different
577 DC precursors may be present in the normal human intestinal LP. However, confirmation of this
578 idea will require formal exploration of progenitor capacity by appropriate methods *in vitro* or *in*
579 *vivo*.
580
581 In the mouse intestine, monocytes differentiate into macrophages through intermediate stages in
582 what is known as the macrophage 'waterfall' (Bain et al., 2013; Rivollier et al., 2012; Schridde et
583 al., 2017; Tamoutounour et al., 2012). It has recently been suggested that a similar monocyte-
584 macrophage differentiation continuum may also exist in the human ileal mucosa (Bujko et al.,
585 2018). In support of this, we identified 11 clusters of Mono/Mac which included classical
586 monocytes, three clusters of mature macrophages, and five clusters which appeared to be
587 intermediate between these. These cells were defined as intermediates due to both expression
588 of genes associated with monocytes and mature macrophage genes, and due to the pseudotime
589 analysis. This concept was also supported by CITE-seq and flow cytometry analyses, which
590 suggested a continuum in which $CD55^{+}$ $CD206^{-}$ $HLA\text{-}DR^{lo}$ monocytes differentiated into $CD55^{+}$
591 $CD206^{-}$ $HLA\text{-}DR^{+}$ early intermediates, $CD55^{-}$ $CD11a^{int}$ $CD206^{+}$ late intermediates, followed by two
592 populations of $CD11a^{-}$ $CD14^{int}$ $CD163^{int}$ and $CD14^{hi}$ $CD163^{hi}$ macrophages. Using this panel we
593 found that the small intestine contains a significantly higher proportion of the $CD14^{int}$ $CD163^{int}$
594 macrophages than the colon. However, a complete definition of these cells as developmentally
595 related will depend on further analysis, such as tracing of donor cells in transplant patients (Bujko
596 et al., 2018). Similarly, while the small *CD163*^{lo} macrophage clusters M9 and M10 transcriptionally
597 resembled self-maintaining and adipose tissue macrophages, respectively, confirmation of these
598 identities will await validation using other methods.
599

Our trajectory analysis suggested that monocytes entering the LP may give rise to two parallel pathways of macrophage development. One pathway (M3-M5-M7) was characterised by clusters expressing higher expression levels of pro-inflammatory cytokines and stimulus response genes, as well as inferred activity of NFκB/TNFa/EGFR signalling pathways and NFκB/ATF/AP-1 transcription factors. The other pathway (M2-M4-M6-M8)) included clusters which were phenotypically and transcriptionally similar to the first, but without expression of the proinflammatory cytokines and without activity of the NFκB/TNFa/EGFR signalling pathways and NFκB/ATF/AP-1 transcription factors. Instead, these clusters showed inferred activity of JAK-STAT and WNT pathways, and of the transcriptional repressor REST. The implications of this are unclear, but it could reflect monocyte-macrophage differentiation occurring within different anatomical or immunological niches in the LP. Work in mice has shown that macrophages in the LP and muscularis layers of the intestine may be distinguished by their pro- or anti-inflammatory phenotype respectively (Gabanyi et al., 2016; Viola and Boeckxstaens, 2020), while a population of $CD169^{+}$ macrophages with pro-inflammatory properties has been described near the crypt base of the LP (Hiemstra et al., 2014). Furthermore, there is increasing evidence from other tissues that monocyte-derived resident macrophages can acquire very different properties depending on the exact niche which they locate to, such as close to nerves, blood vessels or airways (Blériot et al., 2020). In our Mono/Mac clusters, there was heterogeneity in expression of surface markers, efferocytosis genes, cytokines, and inferred activity of signalling pathways and transcription factors. Whether similar anatomical factors constrain the development of these heterogeneous populations of macrophages identified in human intestinal LP remains to be elucidated. We also identified two parallel pathways of monocyte development, with all clusters of one pathway expressing higher levels of pro-inflammatory cytokines than their counterparts in the other pathway. This could suggest that, similar to the situation in mice (Desalegn and Pabst, 2019),

624 monocytes entering the human gut can quickly gain a steady state or a pro-inflammatory
625 phenotype, depending on the local environment.
626
627 Accumulation of pro-inflammatory, $CD14^{+}$ $HLADR^{int}$ cells is a characteristic feature of active
628 inflammatory bowel disease (Jones et al., 2018; Martin et al., 2019) and recent studies have
629 reported single-cell analyses of human intestinal MNP in IBD, as part of total leukocyte analyses
630 (Martin et al., 2019; Rubin et al., 2019; Smillie et al., 2019). However, the number of MNP cells
631 was small in these studies and there was no consensus on the exact nature of these cells, nor
632 how they correspond to putative counterparts in the healthy gut. Here we confirmed the
633 accumulation of $CD14^{+}$ $HLADR^{int}$ monocytes and monocyte-derived intermediates in both colonic
634 and ileal LP during active IBD, along with fewer $CD14^{int}$ and $CD14^{hi}$ macrophages. Late
635 intermediates appeared to expand in response to milder inflammation than monocytes and early
636 intermediates, while monocytes/early intermediates seemed to only expand in more severe
637 inflammation. The failure of monocytes to develop into mature macrophages in inflamed intestine
638 was initially thought to reflect a block during the intermediate stages of differentiation (Bain et al.,
639 2013; Rivollier et al., 2012). However, more recent work in mice has suggested that monocytes
640 begin to follow an alternative pathway of development as soon as they enter the inflamed intestine
641 (Desalegn and Pabst, 2019). Our findings support a model in which monocytes immediately
642 respond to different environments as they enter the gut, and they suggest that this may be
643 occurring constantly in the steady-state intestine. Here we have provided an overview of the
644 developmental trajectory and heterogeneity of monocyte-derived cells in the intestinal LP, and we
645 have identified novel markers which can be used to interrogate these cells.
646
647 In summary, our single-cell studies of MNP in carefully isolated LP emphasise the heterogeneity
648 of these cells in both health and disease, and show that this may also differ depending on the

649 gut segment being examined. By identifying novel genetic and phenotypic markers, our work
650 should provide useful information for further studies of how monocytes, macrophages and DC
651 subsets might contribute to regulation of immune responses in the intestine.
652
653 **Acknowledgments**
654 We thank all patients and collaborating staff at Herlev hospital, and in particular the
655 Gastroenterology Team (Department of Pathology) for help in providing tissue samples.
656 Sequencing was performed at the National Genomics Infrastructure (NGI) and Science for Life
657 Laboratory SNP&SEQ Technology Platform in Uppsala (supported by the Swedish Research
658 Council and the Knut and Alice Wallenberg Foundation). We thank Dr J Rizk (Copenhagen
659 University) for valuable guidance regarding signalling pathways. This work was supported by a
660 grant from the Lundbeck foundation (R155-2014-4184), Denmark, to WW.A and S.B, the Danish
661 Research Council (Sapere Aude III senior researcher grant 1331-00136B to W.W.A), and the
662 Swedish Medical Research Council (2017-02072) and the Swedish Cancerfonden (18 0598) to
663 W.W.A.
664
665
666

667 ***Materials and Methods***

668

669 **Methods**

670 **HUMAN SUBJECTS**

671 Resection samples were taken with informed consent from patients undergoing colorectal cancer
672 surgery, as approved by the Videnskabsetiske Komité for Region Hovedstaden, ethical
673 permission H-3-2013-118. Resection tissues were taken at least 20 cm distant from any tumours
674 present.

675

676 Biopsy samples were obtained with informed consent from adult IBD patients attending routine
677 colonoscopy for initial disease surveillance or ongoing disease assessment (Table S2 for
678 anonymised patient information) at the Western General Hospital, Edinburgh, UK, after informed
679 consent under existing approvals (REC:19/ES/0087). A diagnosis of IBD was made using
680 standard criteria (Leonard-Jones), with all patients part of the Lothian IBD registry (Jones et al.,
681 2019). Endoscopic assessment of disease severity for each biopsy site was performed by
682 clinicians using the Mayo endoscopic subscore for UC or the simple endoscopic score (SES-CD)
683 for CD. Each biopsy site was classed as quiescent, mild, moderate or severe endoscopic activity
684 to enable comparison across IBD subtypes, and 3-5 biopsies were taken for analysis per site.

685

686 **METHOD DETAILS**

687 **Tissue processing**

688 Samples were processed as described previously (Jørgensen et al., 2021). Briefly, resection
689 samples were taken at least 10 cm distant from tumours, where present. The muscularis externa
690 was removed using curved surgical scissors and the remaining tissue was incubated in a 370rpm
691 shaking incubator twice for 10 min at 37°C in RPMI-5 (RPMI/5% FCS/1% penicillin and
692 streptomycin) containing 4 mM DTT, to remove mucus. Macroscopically visible submucosa (SM)

693 was trimmed away using scissors. The mucosa was then separated from the underlying SM under
694 a stereo microscope using forceps. Epithelial cells were removed from the remaining mucosa by
695 shaking four times in $Ca2^{+}$ and $Mg2^{+}$ - free HBSS containing 1% penicillin and streptomycin and
696 5 mM EDTA at 37°C, for 10 min each time. Any remaining ILF present in the mucosa were then
697 dissected out using a scalpel under a stereo microscope with a transmitted light source. The
698 remaining GALT-free LP was cut into 2-4 mm^2 pieces prior to digestion. A single-cell suspension
699 of isolated LP was generated by shaking tissues at 370 rpm in a 37°C incubator in RPMI-5
700 containing 30 µg/ml DNase and 5 mg/ml collagenase D or 2.5 mg/ml Liberase TM for 45 min, at
701 37°C. The suspension was passed through a 100 µm filter before washing twice in fresh media
702 and centrifuging to form a pellet.
703
704 **Flow cytometry**
705 Cell suspensions were stained with the antibodies indicated (Table S3) in Brilliant stain buffer (BD
706 Biosciences) containing 4% normal mouse serum according to standard techniques. The cells
707 were stained with 7-AAD and analyzed on an LSR Fortessa 2 (BD Biosciences) using Flowjo
708 software (Treestar).
709
710 For the Legendscreen assay (Biolegend), each antibody was first resuspended in 35 µl of FACS
711 buffer (PBS with 5% FCS and 0.05% sodium azide). Up to $300x10^6$ cells were stained with the
712 antibody backbone panel (Table S4), washed and resuspended in PBS with 5% FCS. 40 µl of cell
713 suspension was aliquoted into each well of V-bottom 96-well plates containing 10 ul of the PE-
714 conjugated antibody per well. The cells were analysed using an LSR Fortessa 2 with High
715 Throughput Sampler (BD).
716
717 **Magnetic enrichment of MNP**

718 Single-cell suspensions to be used for single-cell sequencing were enriched for HLA-DR$^+$ cells
719 using anti-HLA-DR microbeads (Miltenyi Biotec), as per the manufacturer's instructions. Briefly,
720 cells were counted then centrifuged and resuspended in 80 µl cold MACS buffer (PBS with 0.5%
721 BSA and 2mM EDTA) and 20 µl HLA-DR microbeads, per 1x10^7 total cells. Cells were stored on
722 ice for 15 minutes then washed in 1 ml MACS buffer per 1x10^7 cells. Cells were centrifuged and
723 resuspended in 500 µl fresh MACS buffer before adding to an LS MACS column. The flow-through
724 was discarded and the HLA-DR$^+$ cells were washed through the column with 5 ml fresh buffer.
725
726 **Cell sorting**
727 Cells were counted, pelleted, and stained for flow cytometry as above. The cells were stained
728 with anti-human CD45-BV421, CD3-PECF594, CD19-PECF594, HLA-DR-AF700, and 7-AAD
729 was added before sorting to exclude dead cells. Viable CD45$^+$ HLA-DR$^{int/+}$ CD3$^-$ CD19$^-$ cells were
730 sorted on a FACSMelody sorter (BD) into MACS buffer, before being counted and re-suspended
731 in PBS with 0.4% BSA.
732
733 **CITE-seq**
734 For some samples, cells were first stained with barcode-labelled antibodies together with the
735 antibodies used for sorting, before running the 10x protocol. The Totalseq-A antibodies used were
736 anti-human CD1c (clone L161), CD14 (clone M5E2), CD11a (clone TS2/4), CD55 (clone JS11),
737 CD5 (clone UCHT2), CD206 (clone 15-2), CD209 (clone 9E9A8), and CD11c (clone S-HCL-3),
738 all from Biolegend.
739
740 **Single-cell 10x protocol**
741 Suspensions of sorted single cells were subjected to droplet-based massively parallel single-cell
742 RNA sequencing using the Chromium Single Cell 3′ Reagent Kit v3 following the manufacturer's

743 instructions (10x Genomics). The 10x Chromium Controller generated nanoliter-scale Gel Bead-
744 In Emulsions (GEMs) droplets, where each cell was labeled with a specific barcode, and each
745 transcript labeled with a unique molecular identifier (UMI). After reverse transcription (55°C for
746 45min and 85 °C for 5min), the GEMs were broken down and the barcoded cDNA was purified
747 with Dynabeads MyOne Silane beads (Thermofisher). The cDNA was amplified by PCR with 10x
748 genomics and ADT additive primer (98 °C for 3min; 12 cycles of 98 °C for 15sec, 67 °C for 20sec
749 and 72 °C for 1; 72 °C for 1min, end at 4 °C). The products were size separated with SPRIselect
750 beads (Beckman Coulter) into fragments < 300nt containing antibody derived tags (ADTs) and >
751 300nt containing cDNAs derived from cellular mRNA.
752
753 For sc-RNA libraries, 50 ng of amplified cDNA was used for final library preparation, consisting of
754 enzymatic fragmentation, end repair, A-tailing, adaptor ligation and sample index PCR as per the
755 manufacturer's instructions.
756
757 For epitope sequencing (CITE-seq), 2ul of ADTs were PCR amplified with Illumina compatible SI
758 PCR and TrueSeq Small RNA RPIx primers (15 cycles). Final libraries were purified using
759 SPRIselect beads.
760 Quality and quantity of the final libraries (sc-RNA and ADT) were measured using the Agilent
761 2100 Bioanalyzer equipped with High Sensitivity DNA chip. Libraries were pooled according to
762 the starting number of cells of each run (10% ADT + 90% sc-RNA).
763
764 SI-PCR primer: AATGATACGGCGACCACCGAGATCTACACTCTTTCCCTACACGACGC*T*C
765 ADT additive primer: CCTTGGCACCCGAGAATT*C*C
766 RPI1:CAAGCAGAAGACGGCATACGAGATCGTGATGTGACTGGAGTTCCTTGGCACCCGAG
767 AATTC*C*A

768 RPI2:CAAGCAGAAGACGGCATACGAGATACATCGGTGACTGGAGTTCCTTGGCACCCGAG
769 AATTC*C*A
770 RPI3:CAAGCAGAAGACGGCATACGAGATGCCTAAGTGACTGGAGTTCCTTGGCACCCGAG
771 AATTC*C*A
772 RPI4:CAAGCAGAAGACGGCATACGAGATTGGTCAGTGACTGGAGTTCCTTGGCACCCGAG
773 AATTC*C*A
774 * indicates a phosphorothioate bond
775
776 **Sequencing**
777 Illumina sequencing was carried out at the Genomics Core Unit: Center of Excellence for
778 Fluorescent Bioanalytics (KFB, University of Regensburg, Germany) and at the SNP&SEQ
779 Technology Platform in Sweden which is part of the National Genomics Infrastructure (NGI),
780 funded by the Swedish Council for Research Infrastructures and Science for Life Laboratory.
781 Libraries were sequenced using HiSeq, NextSeq and NovaSeq systems (300 cycles), targeting a
782 minimum of 30,000 read pairs per cell for sc-RNA and 3000 read pairs per cell for ADTs.
783
784
785 **Bioinformatic analysis**
786 Sequencing data was pre-processed and aligned with CellRanger (version 2.2.0 for the first
787 patient samples and version 3.1.0 for all other samples)(Dobin et al., 2013; Zheng et al., 2017).
788 The sequencing data from the samples stained with TotalSeq antibodies was processed with cite-
789 seq count (Stoeckius et al., 2017). Each sample was then read into a Seurat (version 3.1.5) (Stuart
790 et al., 2019) object in R (versions 3.5.1/4.0.1) (R Core Team, 2018) and processed by removing
791 cells with exceptionally low or high UMI and gene counts (debris and doublets). The lower
792 thresholds were set from 500-1000 genes per cell and the upper threshold were set from 3000-

6000. Furthermore, cells with mitochondrial gene content > 10% were also removed. The thresholds were set by studying UMI and gene counts, and mitochondrial gene content according to current best practise (Luecken and Theis, 2019). The debris removed from each sample was used as empty droplet information to normalize the protein level in the individual samples together with the isotype controls(Mulè et al., 2020). The normalized protein data was added to each of the relevant samples.

The scRNA data for each sample was normalized and cell cycle gene modules were calculated using the Seurat CellCycleScoring function and additionally a gene module representing cell cycle genes from the tool ccRemover by summing the raw counts of these genes per cell divided by the total number of reads per cell(Barron and Li, 2016). The top 3000 most variable genes were identified with the selection method vst.

After this initial data processing, all the samples were integrated with Seurat anchor integration and gene expression was scaled while regressing out effect of cell cycle, UMI counts, and mitochondrial gene content. The merged data were dimensionality reduced with PCA and the 15 first PCs were chosen for downstream analysis. A shared nearest neighbour graph was constructed and used to cluster the data with Louvain clustering. The PCs were also used to dimensionality reduce the data further with UMAP for visulization purposes. The data were reclustered on described populations after removal of contaminating cell types and new UMAPs calculated.

The pseudobulk for heatmaps and PCA was performed with the Seurat AverageExpression function. The PCA on pseudobulk of clusters was performed only on genes from published gene signatures of blood DC2, blood monocytes and in vitro mo-Macs(Tang-Huau et al., 2018). Differential gene expression was calculated with Seurat FindMarkers for comparisons between

specific groups or FindAllMarkers for DEGs for all clusters both using the standard non-parameteric Wilcoxon rank sum test.

Trajectory inference was performed with tSPACE on PC spaces of indicated populations (Dermadi et al., 2020). The outputs were further dimensionality reduced with UMAP(Becht et al., 2019; McInnes et al., 2018) to 2 and 3 dimensions with distance metric set to Pearson. Clustering was performed with Louvain clustering for Seurat on the tSPACE PC output as input. RNA velocity estimates were calculated for T=1 and only included genes with splicing information also present in the variable genes and only on cells of interest (e.g. precursors). The information was embedded on top of 2D UMAPs from the tSPACE trajectories using n=400, scale=sqrt, grid.n=50 and arrow.scale=2 (La Manno et al., 2018).

The data set from (Bourdely et al., 2020) was downloaded and processed as described in the methods section of that study. The blood data were then integrated with matching cell types from the lamina propria (identified monocytes and DC2-like cells) and differentially expressed genes were identified between tissues in each matching cell type.

QUANTIFICATION AND STATISTICAL ANALYSIS

Flow cytometry analyses were performeddata were analysed using in Prism software (GraphPad). Details for, with the statistical tests used in each experiment can be foundbeing shown in the relevant figure legends. Statistical significance was defined as *p<0.05, **p<0.01, ***p<0.001. Statistical analysis of sequencing data was performed in R as described in the bioinformatics section above.

References

Arroyo Portilla, C., Tomas, J., Gorvel, J., and Lelouard, H. (2021). From Species to Regional and Local Specialization of Intestinal Macrophages. Front. Cell Dev. Biol. *8*.

Bahrami, S., and Drabløs, F. (2016). Gene regulation in the immediate-early response process. Adv. Biol. Regul. *62*, 37–49.

Bain, C.C., and Schridde, A. (2018). Origin, differentiation, and function of intestinal macrophages. Front. Immunol. *9*, 1–15.

Bain, C.C., Scott, C.L., Uronen-Hansson, H., Gudjonsson, S., Jansson, O., Grip, O., Guilliams, M., Malissen, B., Agace, W.W., and Mowat, a M. (2013). Resident and pro-inflammatory macrophages in the colon represent alternative context-dependent fates of the same Ly6Chi monocyte precursors. Mucosal Immunol. *6*, 498–510.

Bain, C.C., Bravo-Blas, A., Scott, C.L., Perdiguero, E.G., Geissmann, F., Henri, S., Malissen, B., Osborne, L.C., Artis, D., and Mowat, A.M. (2014). Constant replenishment from circulating monocytes maintains the macrophage pool in the intestine of adult mice. Nat. Immunol. *15*.

Balan, S., Arnold-Schrauf, C., Abbas, A., Couespel, N., Savoret, J., Imperatore, F., Villani, A.C., Vu Manh, T.P., Bhardwaj, N., and Dalod, M. (2018). Large-Scale Human Dendritic Cell Differentiation Revealing Notch-Dependent Lineage Bifurcation and Heterogeneity. Cell Rep. *24*, 1902-1915.e6.

Barone, F., Vossenkamper, A., Boursier, L., Su, W., Watson, A., John, S., Dunn-Walters, D.K., Fields, P., Wijetilleka, S., Edgeworth, J.D., et al. (2011). IgA-producing plasma cells originate from germinal centers that are induced by B-cell receptor engagement in humans. Gastroenterology *140*, 947–956.

Barron, M., and Li, J. (2016). Identifying and removing the cell-cycle effect from single-cell RNA-Sequencing data. Sci. Rep. *6*, 33892.

Becht, E., McInnes, L., Healy, J., Dutertre, C.-A., Kwok, I.W.H., Ng, L.G., Ginhoux, F., and Newell, E.W. (2019). Dimensionality reduction for visualizing single-cell data using UMAP. Nat. Biotechnol. *37*, 38–44.

Bernardo, D., Durant, L., Mann, E.R., Bassity, E., Montalvillo, E., Man, R., Vora, R., Reddi, D., Bayiroglu, F., Fernández-Salazar, L., et al. (2016). Chemokine (C-C Motif) Receptor 2 Mediates Dendritic Cell Recruitment to the Human Colon but Is Not Responsible for Differences Observed in Dendritic Cell Subsets, Phenotype, and Function Between the Proximal and Distal Colon. Cell. Mol. Gastroenterol. Hepatol. *2*, 22-39.e5.

Bernardo, D., Chaparro, M., and Gisbert, J.P. (2018). Human Intestinal Dendritic Cells in Inflammatory Bowel Diseases. Mol. Nutr. Food Res. *62*, 1–8.

Blériot, C., Chakarov, S., and Ginhoux, F. (2020). Determinants of Resident Tissue Macrophage Identity and Function. Immunity *52*, 957–970.

Bogunovic, M., Ginhoux, F., Helft, J., Shang, L., Hashimoto, D., Greter, M., Liu, K., Jakubzick, C., Ingersoll, M. a, Leboeuf, M., et al. (2009). Origin of the lamina propria dendritic cell network. Immunity *31*, 513–525.

Bourdely, P., Anselmi, G., Vaivode, K., Ramos, R.N., Missolo-Koussou, Y., Hidalgo, S., Tosselo, J., Nuñez, N., Richer, W., Vincent-Salomon, A., et al. (2020). Transcriptional and Functional Analysis of CD1c+ Human Dendritic Cells Identifies a CD163+ Subset Priming CD8+CD103+ T Cells. Immunity *53*, 335-352.e8.

Boursier, L., Gordon, J.N., Thiagamoorthy, S., Edgeworth, J.D., and Spencer, J. (2005). Human Intestinal IgA Response Is Generated in the Organized Gut-Associated Lymphoid Tissue but Not in the Lamina Propria. Gastroenterology *128*, 1879–1889.

Breton, G., Lee, J., Zhou, Y.J., Schreiber, J.J., Keler, T., Puhr, S., Anandasabapathy, N., Schlesinger, S., Caskey, M., Liu, K., et al. (2015). Circulating precursors of human CD1c+ and CD141+ dendritic cells. J. Exp. Med. *212*, 401–413.

Brown, C.C., Gudjonson, H., Pritykin, Y., Deep, D., Lavallée, V.P., Mendoza, A., Fromme, R., Mazutis, L., Ariyan, C., Leslie, C., et al. (2019). Transcriptional Basis of Mouse and Human Dendritic Cell Heterogeneity. Cell *179*, 846-863.e24.

Bujko, A., Atlasy, N., Landsverk, O.J.B., Richter, L., Yaqub, S., Horneland, R., Øyen, O., Aandahl, E.M., Aabakken, L., Stunnenberg, H.G., et al. (2018). Transcriptional and functional profiling defines human small intestinal macrophage subsets. J. Exp. Med. *215*, 441–458.

Cabeza-Cabrerizo, M., Cardoso, A., Minutti, C.M., Pereira da Costa, M., and Reis E Sousa, C. (2021). Dendritic Cells Revisited. Annu. Rev. Immunol. 131–166.

Caër, C., and Wick, M.J. (2020). Human Intestinal Mononuclear Phagocytes in Health and Inflammatory Bowel Disease. Front. Immunol. *11*, 410.

Carlin, L.M., Stamatiades, E.G., Auffray, C., Hanna, R.N., Glover, L., Vizcay-Barrena, G., Hedrick, C.C., Cook, H.T., Diebold, S., and Geissmann, F. (2013). Nr4a1-dependent Ly6C(low) monocytes monitor endothelial cells and orchestrate their disposal. Cell *153*, 362–375.

Carpentier, S., Vu Manh, T.P., Chelbi, R., Henri, S., Malissen, B., Haniffa, M., Ginhoux, F., and Dalod, M. (2016). Comparative genomics analysis of mononuclear phagocyte subsets confirms homology between lymphoid tissue-resident and dermal XCR1+ DCs in mouse and human and distinguishes them from Langerhans cells. J. Immunol. Methods *432*, 35–49.

Chapuy, L., Bsat, M., Sarkizova, S., Rubio, M., Therrien, A., Wassef, E., Bouin, M., Orlicka, K., Weber, A., Hacohen, N., et al. (2019). Two distinct colonic CD14+ subsets characterized by single-cell RNA profiling in Crohn's disease. Mucosal Immunol. *12*, 703–719.

Chen, J., Schlitzer, A., Chakarov, S., Ginhoux, F., and Poidinger, M. (2016). Mpath maps multi-branching single-cell trajectories revealing progenitor cell progression during development. Nat. Commun. *7*, 11988.

Cytlak, U., Resteu, A., Pagan, S., Green, K., Milne, P., Maisuria, S., McDonald, D., Hulme, G., Filby, A., Carpenter, B., et al. (2020). Differential IRF8 Transcription Factor Requirement Defines Two Pathways of Dendritic Cell Development in Humans. Immunity *53*, 353-370.e8.

Dermadi, D., Bscheider, M., Bjegovic, K., Lazarus, N.H., Szade, A., Hadeiba, H., and Butcher, E.C. (2020). Exploration of Cell Development Pathways through High-Dimensional Single Cell Analysis in Trajectory Space. IScience *23*, 100842.

Desalegn, G., and Pabst, O. (2019). Inflammation triggers immediate rather than progressive changes in monocyte differentiation in the small intestine. Nat. Commun. *10*, 3229.

Dobin, A., Davis, C.A., Schlesinger, F., Drenkow, J., Zaleski, C., Jha, S., Batut, P., Chaisson, M., and Gingeras, T.R. (2013). STAR: ultrafast universal RNA-seq aligner. Bioinformatics *29*, 15–21.

Durand, M., Walter, T., Pirnay, T., Naessens, T., Gueguen, P., Goudot, C., Lameiras, S., Chang, Q., Talaei, N., Ornatsky, O., et al. (2019). Human lymphoid organ cDC2 and macrophages play complementary roles in T follicular helper responses. J. Exp. Med. *216*, 1561–1581.

Dutertre, C.A., Becht, E., Irac, S.E., Khalilnezhad, A., Narang, V., Khalilnezhad, S., Ng, P.Y., van den Hoogen, L.L., Leong, J.Y., Lee, B., et al. (2019). Single-Cell Analysis of Human Mononuclear Phagocytes Reveals Subset-Defining Markers and Identifies Circulating Inflammatory Dendritic Cells. Immunity *51*, 573-589.e8.

Elliott, M.R., Koster, K.M., and Murphy, P.S. (2017). Efferocytosis Signaling in the Regulation of Macrophage Inflammatory Responses. J. Immunol. *198*, 1387–1394.

Fenton, T.M., Jørgensen, P.B., Niss, K., Rubin, S.J.S., Mörbe, U.M., Riis, L.B., Da Silva, C., Plumb, A., Vandamme, J., Jakobsen, H.L., et al. (2020). Immune Profiling of Human Gut-Associated Lymphoid Tissue Identifies a Role for Isolated Lymphoid Follicles in Priming of Region-Specific Immunity. Immunity *52*, 557-570.e6.

Frey, S.K., and Vogel, S. (2011). Vitamin A Metabolism and Adipose Tissue Biology. Nutrients *3*, 27–39.

Gabanyi, I., Muller, P.A., Feighery, L., Oliveira, T.Y., Costa-Pinto, F. a., and Mucida, D. (2016). Neuro-immune Interactions Drive Tissue Programming in Intestinal Macrophages. Cell *164*, 378–391.

Garcia-Alonso, L., Holland, C.H., Ibrahim, M.M., Turei, D., and Saez-Rodriguez, J. (2019). Benchmark and integration of resources for the estimation of human transcription factor activities. Genome Res.

Girard, M., Law, J.C., Edilova, M.I., and Watts, T.H. (2020). Type I interferons drive the maturation of human DC3s with a distinct costimulatory profile characterized by high GITRL. Sci. Immunol. *5*, eabe0347.

Goudot, C., Coillard, A., Villani, A.C., Gueguen, P., Cros, A., Sarkizova, S., Tang-Huau, T.L., Bohec, M., Baulande, S., Hacohen, N., et al. (2017). Aryl Hydrocarbon Receptor Controls Monocyte Differentiation into Dendritic Cells versus Macrophages. Immunity *47*, 582-596.e6.

Grajales-Reyes, G.E., Iwata, A., Albring, J., Wu, X., Tussiwand, R., KC, W., Kretzer, N.M., Briseño, C.G., Durai, V., Bagadia, P., et al. (2015). Batf3 maintains autoactivation of Irf8 for commitment of a CD8α+ conventional DC clonogenic progenitor. Nat. Immunol. *16*, 708–717.

Guilliams, M., Dutertre, C.-A., Scott, C.L., McGovern, N., Sichien, D., Chakarov, S., Van Gassen, S., Chen, J., Poidinger, M., De Prijck, S., et al. (2016). Unsupervised High-Dimensional Analysis Aligns Dendritic Cells across Tissues and Species. Immunity *45*, 669–684.

Habtezion, A., Nguyen, L.P., Hadeiba, H., and Butcher, E.C. (2016). Leukocyte Trafficking to the Small Intestine and Colon. Gastroenterology *150*, 340–354.

Hiemstra, I.H., Beijer, M.R., Veninga, H., Vrijland, K., Borg, E.G.F., Olivier, B.J., Mebius, R.E., Kraal, G., and Den Haan, J.M.M. (2014). The identification and developmental requirements of colonic CD169+ macrophages. Immunology *142*, 269–278.

Holland, C.H., Tanevski, J., Perales-Patón, J., Gleixner, J., Kumar, M.P., Mereu, E., Joughin, B.A., Stegle, O., Lauffenburger, D.A., Heyn, H., et al. (2020). Robustness and applicability of transcription factor and pathway analysis tools on single-cell RNA-seq data. Genome Biol. *21*, 36.

Honda, M., Surewaard, B.G.J., Watanabe, M., Hedrick, C.C., Lee, W.-Y., Brown, K., McCoy, K.D., and Kubes, P. (2020). Perivascular localization of macrophages in the intestinal mucosa is regulated by Nr4a1 and the microbiome. Nat. Commun. *11*, 1329.

Jaensson, E., Uronen-Hansson, H., Pabst, O., Eksteen, B., Tian, J., Coombes, J.L., Berg, P.-L., Davidsson, T., Powrie, F., Johansson-Lindbom, B., et al. (2008). Small intestinal CD103+ dendritic cells display unique functional properties that are conserved between mice and humans. J. Exp. Med. *205*, 2139–2149.

Joeris, T., Müller-Luda, K., Agace, W.W., and Mowat, A.M. (2017). Diversity and functions of intestinal mononuclear phagocytes. Mucosal Immunol. 1–20.

Jones, G.-R., Bain, C.C., Fenton, T.M., Kelly, A., Brown, S.L., Ivens, A.C., Travis, M.A., Cook, P.C., and MacDonald, A.S. (2018). Dynamics of Colon Monocyte and Macrophage Activation During Colitis. Front. Immunol. *9*.

Jones, G.-R., Lyons, M., Plevris, N., Jenkinson, P.W., Bisset, C., Burgess, C., Din, S., Fulforth, J., Henderson, P., Ho, G.-T., et al. (2019). IBD prevalence in Lothian, Scotland, derived by capture-recapture methodology. Gut gutjnl-2019-318936.

Jørgensen, P.B., Fenton, T.M., Mörbe, U.M., Riis, L.B., Jakobsen, H.L., Nielsen, O.H., and Agace, W.W. (2021). Identification, isolation and analysis of human gut-associated lymphoid tissues. Nat. Protoc.

Joshi, H.R., Hill, H.R., Zhou, Z., He, X., Voelkerding, K. V., and Kumánovics, A. (2020). Frontline Science: Cxxc5 expression alters cell cycle and myeloid differentiation of mouse hematopoietic stem and progenitor cells. J. Leukoc. Biol. *108*, 469–484.

Kang, B., Alvarado, L.J., Kim, T., Lehmann, M.L., Cho, H., He, J., Li, P., Kim, B.H., Larochelle, A., and Kelsall, B.L. (2020). Commensal microbiota drive the functional diversification of colon

macrophages. Mucosal Immunol. *13*, 216–229.
Koeva, M., Forsberg, E.C., and Stuart, J.M. (2011). Computational Integration of Homolog and Pathway Gene Module Expression Reveals General Stemness Signatures. PLoS One *6*, e18968.
Lantz, C., Radmanesh, B., Liu, E., Thorp, E.B., and Lin, J. (2020). Single-cell RNA sequencing uncovers heterogenous transcriptional signatures in macrophages during efferocytosis. Sci. Rep. *10*, 14333.
Li, Y., Yun, K., and Mu, R. (2020). A review on the biology and properties of adipose tissue macrophages involved in adipose tissue physiological and pathophysiological processes. Lipids Health Dis. *19*, 1–9.
Lim, K.P.H., Milne, P., Poidinger, M., Duan, K., Lin, H., McGovern, N., Abhyankar, H., Zinn, D., Burke, T.M., Eckstein, O.S., et al. (2020). Circulating CD1c+ myeloid dendritic cells are potential precursors to LCH lesion CD1a+CD207+ cells. Blood Adv. *4*, 87–99.
Luecken, M.D., and Theis, F.J. (2019). Current best practices in single-cell RNA-seq analysis: a tutorial. Mol. Syst. Biol. *15*.
Ma, W., Lee, J., Backenroth, D., Zhou, Y.J., Bush, E., Sims, P., Liu, K., and Shen, Y. (2019). Single cell RNA-Seq reveals pre-cDCs fate determined by transcription factor combinatorial dose. BMC Mol. Cell Biol. *20*, 1–14.
Maixner, N., Pecht, T., Haim, Y., Chalifa-Caspi, V., Goldstein, N., Tarnovscki, T., Liberty, I.F., Kirshtein, B., Golan, R., Berner, O., et al. (2020). A trail-tl1a paracrine network involving adipocytes, macrophages, and lymphocytes induces adipose tissue dysfunction downstream of e2f1 in human obesity. Diabetes *69*, 2310–2323.
Mann, E.R., Bernardo, D., English, N.R., Landy, J., Al-Hassi, H.O., Peake, S.T., Man, R., Elliott, T.R., Spranger, H., Lee, G.H., et al. (2015). Compartment-specific immunity in the human gut: properties and functions of dendritic cells in the colon versus the ileum. Gut *140*, 169.
La Manno, G., Soldatov, R., Zeisel, A., Braun, E., Hochgerner, H., Petukhov, V., Lidschreiber, K., Kastriti, M.E., Lönnerberg, P., Furlan, A., et al. (2018). RNA velocity of single cells. Nature *560*, 494–498.
Martin, J.C., Chang, C., Boschetti, G., Ungaro, R., Giri, M., Grout, J.A., Gettler, K., Chuang, L. shiang, Nayar, S., Greenstein, A.J., et al. (2019). Single-Cell Analysis of Crohn's Disease Lesions Identifies a Pathogenic Cellular Module Associated with Resistance to Anti-TNF Therapy. Cell *178*, 1493-1508.e20.
Masahata, K., Umemoto, E., Kayama, H., Kotani, M., Nakamura, S., Kurakawa, T., Kikuta, J., Gotoh, K., Motooka, D., Sato, S., et al. (2014). Generation of colonic IgA-secreting cells in the caecal patch. Nat. Commun. *5*, 3704.
McInnes, L., Healy, J., Saul, N., and Großberger, L. (2018). UMAP: Uniform Manifold Approximation and Projection. J. Open Source Softw.
Miller, J.C., Brown, B.D., Shay, T., Gautier, E.L., Jojic, V., Cohain, A., Pandey, G., Leboeuf, M., Elpek, K.G., Helft, J., et al. (2012). Deciphering the transcriptional network of the dendritic cell lineage. Nat. Immunol. *13*, 888–899.
De Monte, A., Olivieri, C.V., Vitale, S., Bailleux, S., Castillo, L., Giordanengo, V., Maryanski, J.L., Segura, E., and Doglio, A. (2016). CD1c-related DCs that express CD207/langerin, but are distinguishable from Langerhans cells, are consistently present in human tonsils. Front. Immunol. *7*, 1–10.
Mörbe, U.M., Jørgensen, P.B., Fenton, T.M., von Burg, N., Riis, L.B., Spencer, J., and Agace, W.W. (2021). Human gut-associated lymphoid tissues (GALT); diversity, structure, and function. Mucosal Immunol.
Mowat, A.M., and Agace, W.W. (2014). Regional specialization within the intestinal immune system. Nat. Rev. Immunol. *14*, 667–685.
Mulè, M., Martins, A., and Tsang, J. (2020). Normalizing and denoising protein expression data

from droplet-based single cell profiling. Preprint.
Na, Y.R., Stakenborg, M., Seok, S.H., and Matteoli, G. (2019). Macrophages in intestinal inflammation and resolution: a potential therapeutic target in IBD. Nat. Rev. Gastroenterol. Hepatol. *16*, 531–543.
Ohnmacht, C., Pullner, A., King, S.B.S., Drexler, I., Meier, S., Brocker, T., and Voehringer, D. (2009). Constitutive ablation of dendritic cells breaks self-tolerance of CD4 T cells and results in spontaneous fatal autoimmunity. J. Exp. Med. *206*, 549–559.
Pepe, G., Locati, M., Della Torre, S., Mornata, F., Cignarella, A., Maggi, A., and Vegeto, E. (2018). The estrogen-macrophage interplay in the homeostasis of the female reproductive tract. Hum. Reprod. Update *24*, 652–672.
R Core Team (2018). R: A Language and Environment for Statistical Computing.
Rivollier, A., He, J., Kole, A., Valatas, V., and Kelsall, B.L. (2012). Inflammation switches the differentiation program of Ly6Chi monocytes from antiinflammatory macrophages to inflammatory dendritic cells in the colon. J. Exp. Med. *209*, 139–155.
Rubin, S.J.S., Bai, L., Haileselassie, Y., Garay, G., Yun, C., Becker, L., Streett, S.E., Sinha, S.R., and Habtezion, A. (2019). Mass cytometry reveals systemic and local immune signatures that distinguish inflammatory bowel diseases. Nat. Commun. *10*, 2686.
Sallusto, F., and Lanzavecchia, A. (1994). Efficient presentation of soluble antigen by cultured human dendritic cells is maintained by granulocyte/macrophage colony-stimulating factor plus interleukin 4 and downregulated by tumor necrosis factor alpha. J. Exp. Med. *179*, 1109–1118.
Satpathy, A.T., Kc, W., Albring, J.C., Edelson, B.T., Kretzer, N.M., Bhattacharya, D., Murphy, T.L., and Murphy, K.M. (2012). Zbtb46 expression distinguishes classical dendritic cells and their committed progenitors from other immune lineages. J. Exp. Med. *209*, 1135–1152.
De Schepper, S., Verheijden, S., Aguilera-Lizarraga, J., Viola, M.F., Boesmans, W., Stakenborg, N., Voytyuk, I., Smidt, I., Boeckx, B., Dierckx de Casterlé, I., et al. (2018). Self-Maintaining Gut Macrophages Are Essential for Intestinal Homeostasis. Cell *175*, 400-415.e13.
Schleier, L., Wiendl, M., Heidbreder, K., Binder, M.T., Atreya, R., Rath, T., Becker, E., Schulz-Kuhnt, A., Stahl, A., Schulze, L. Lou, et al. (2020). Non-classical monocyte homing to the gut via α4β7 integrin mediates macrophage-dependent intestinal wound healing. Gut *69*, 252–263.
Schlitzer, A., McGovern, N., and Ginhoux, F. (2015). Dendritic cells and monocyte-derived cells: Two complementary and integrated functional systems. Semin. Cell Dev. Biol. *41*, 9–22.
Schridde, A., Bain, C.C., Mayer, J.U., Montgomery, J., Pollet, E., Denecke, B., Milling, S.W.F., Jenkins, S.J., Dalod, M., Henri, S., et al. (2017). Tissue-specific differentiation of colonic macrophages requires TGFβ receptor-mediated signaling. Mucosal Immunol. 1–13.
Schubert, M., Klinger, B., Klünemann, M., Sieber, A., Uhlitz, F., Sauer, S., Garnett, M.J., Blüthgen, N., and Saez-Rodriguez, J. (2018). Perturbation-response genes reveal signaling footprints in cancer gene expression. Nat. Commun. *9*, 20.
See, P., Dutertre, C.-A., Chen, J., Günther, P., McGovern, N., Irac, S.E., Gunawan, M., Beyer, M., Händler, K., Duan, K., et al. (2017). Mapping the human DC lineage through the integration of high-dimensional techniques. Science (80-.). *356*, eaag3009.
Senda, T., Dogra, P., Granot, T., Furuhashi, K., Snyder, M.E., Carpenter, D.J., Szabo, P.A., Thapa, P., Miron, M., and Farber, D.L. (2019). Microanatomical dissection of human intestinal T-cell immunity reveals site-specific changes in gut-associated lymphoid tissues over life. Mucosal Immunol. *12*, 378–389.
Shaw, T.N., Houston, S.A., Wemyss, K., Bridgeman, H.M., Barbera, T.A., Zangerle-Murray, T., Strangward, P., Ridley, A.J.L., Wang, P., Tamoutounour, S., et al. (2018). Tissue-resident macrophages in the intestine are long lived and defined by Tim-4 and CD4 expression. J. Exp. Med. *215*, 1507–1518.
Silva, H.M., Kitoko, J.Z., and Queiroz, C.P. (2021). c-MAF dependent perivascular macrophages regulate diet induced metabolic syndrome. Preprint.

Smillie, C.S., Biton, M., Ordovas-Montanes, J., Sullivan, K.M., Burgin, G., Graham, D.B., Herbst, R.H., Rogel, N., Slyper, M., Waldman, J., et al. (2019). Intra- and Inter-cellular Rewiring of the Human Colon during Ulcerative Colitis. Cell *178*, 714-730.e22.

Spencer, J., Siu, J.H.Y., and Montorsi, L. (2019). Human intestinal lymphoid tissue in time and space. Mucosal Immunol. *12*, 296–298.

Stoeckius, M., Hafemeister, C., Stephenson, W., Houck-Loomis, B., Chattopadhyay, P.K., Swerdlow, H., Satija, R., and Smibert, P. (2017). Simultaneous epitope and transcriptome measurement in single cells. Nat. Methods.

Stuart, T., Butler, A., Hoffman, P., Hafemeister, C., Papalexi, E., Mauck, W.M., Hao, Y., Stoeckius, M., Smibert, P., and Satija, R. (2019). Comprehensive Integration of Single-Cell Data. Cell *177*, 1888-1902.e21.

T'Jonck, W., Guilliams, M., and Bonnardel, J. (2018). Niche signals and transcription factors involved in tissue-resident macrophage development. Cell. Immunol. *330*, 43–53.

Tamoutounour, S., Henri, S., Lelouard, H., de Bovis, B., de Haar, C., van der Woude, C.J., Woltman, A.M., Reyal, Y., Bonnet, D., Sichien, D., et al. (2012). CD64 distinguishes macrophages from dendritic cells in the gut and reveals the Th1-inducing role of mesenteric lymph node macrophages during colitis. Eur. J. Immunol. *42*, 3150–3166.

Tang-Huau, T.L., and Segura, E. (2019). Human in vivo-differentiated monocyte-derived dendritic cells. Semin. Cell Dev. Biol. *86*, 44–49.

Tang-Huau, T.-L., Gueguen, P., Goudot, C., Durand, M., Bohec, M., Baulande, S., Pasquier, B., Amigorena, S., and Segura, E. (2018). Human in vivo-generated monocyte-derived dendritic cells and macrophages cross-present antigens through a vacuolar pathway. Nat. Commun. *9*, 2570.

Thorén, L.A., Liuba, K., Bryder, D., Nygren, J.M., Jensen, C.T., Qian, H., Antonchuk, J., and Jacobsen, S.-E.W. (2008). Kit Regulates Maintenance of Quiescent Hematopoietic Stem Cells. J. Immunol.

Travis, M.A., Reizis, B., Melton, A.C., Masteller, E., Tang, Q., Proctor, J.M., Wang, Y., Bernstein, X., Huang, X., Reichardt, L.F., et al. (2007). Loss of integrin alpha(v)beta8 on dendritic cells causes autoimmunity and colitis in mice. Nature *449*, 361–365.

Varol, C., Vallon-Eberhard, A., Elinav, E., Aychek, T., Shapira, Y., Luche, H., Fehling, H.J., Hardt, W.-D., Shakhar, G., and Jung, S. (2009). Intestinal lamina propria dendritic cell subsets have different origin and functions. Immunity *31*, 502–512.

Villablanca, E.J., De Calisto, J., Paredes, P.T., Cassani, B., Nguyen, D.D., Gabrielsson, S., and Mora, J.R. (2014). B7 Integrins Are Required To Give Rise To Intestinal Mononuclear Phagocytes With Tolerogenic Potential. Gut *63*, 1431–1440.

Villani, A.-C., Satija, R., Reynolds, G., Sarkizova, S., Shekhar, K., Fletcher, J., Griesbeck, M., Butler, A., Zheng, S., Lazo, S., et al. (2017). Single-cell RNA-seq reveals new types of human blood dendritic cells, monocytes, and progenitors. Science (80-.). *356*, eaah4573.

Villar, J., and Segura, E. (2020). Decoding the Heterogeneity of Human Dendritic Cell Subsets. Trends Immunol. *41*, 1062–1071.

Viola, M.F., and Boeckxstaens, G. (2020). Intestinal resident macrophages: Multitaskers of the gut. Neurogastroenterol. Motil. *32*.

Watchmaker, P.B., Lahl, K., Lee, M., Baumjohann, D., Morton, J., Kim, S.J., Zeng, R., Dent, A., Ansel, K.M., Diamond, B., et al. (2014). Comparative transcriptional and functional profiling defines conserved programs of intestinal DC differentiation in humans and mice. Nat. Immunol. *15*, 98–108.

Worbs, T., Bode, U., Yan, S., Hoffmann, M.W., Hintzen, G., Bernhardt, G., Förster, R., and Pabst, O. (2006). Oral tolerance originates in the intestinal immune system and relies on antigen carriage by dendritic cells. J. Exp. Med. *203*, 519–527.

Yin, X., Yu, H., Jin, X., Li, J., Guo, H., Shi, Q., Yin, Z., Xu, Y., Wang, X., Liu, R., et al. (2017).

Human Blood CD1c + Dendritic Cells Encompass CD5 high and CD5 low Subsets That Differ Significantly in Phenotype, Gene Expression, and Functions. J. Immunol. *198*, 1553–1564.

Zheng, G.X.Y., Terry, J.M., Belgrader, P., Ryvkin, P., Bent, Z.W., Wilson, R., Ziraldo, S.B., Wheeler, T.D., McDermott, G.P., Zhu, J., et al. (2017). Massively parallel digital transcriptional profiling of single cells. Nat. Commun. *8*, 14049.

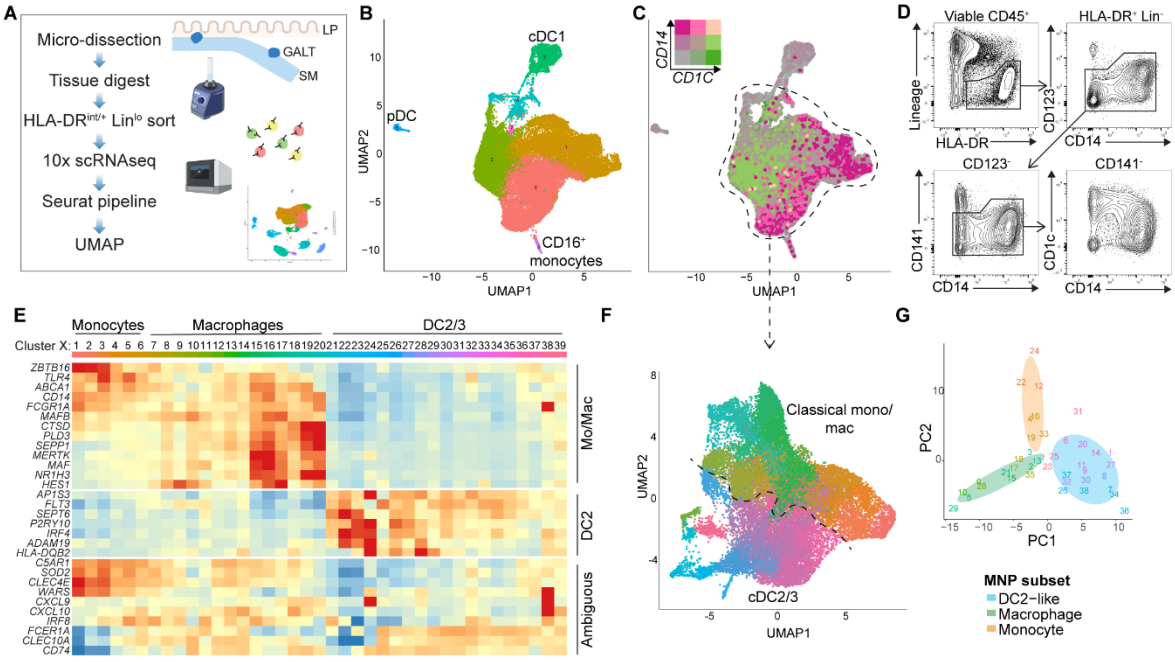

Fig 1 – Untangling intestinal monocytes and macrophages from transcriptionally similar dendritic cells
A-C) scRNAseq analysis of 28,758 combined ileal and colonic LP cells, identified as MNP clusters by high average expression of MHCII genes. n = 6 colonic and 4 paired ileal CRC patient samples.
A) scRNAseq experimental outline
B) UMAP of HLADR+ cell clusters with known cell identities. Dashed line encompasses MNP subsets which are not readily identifiable as pDC, cDC1, or non-classical monocytes. Coloured by Louvain clustering.
C) UMAP of normalized gene co-expression of *CD1C* and *CD14* co-expression.
D) Representative flow cytometry gating strategy to identify *CD1C*$^+$/*CD14*$^+$ MNP in colon LP
E-G) scRNAseq data of 26,578 combined ileal and colonic LP cells identified by expression of *CD1C* and/or *CD14*. n = 6 colonic and 4 paired ileal CRC patient samples
E) Curated heatmap of re-clustered *CD1C*$^+$/*CD14*$^+$ cells showing expression of macrophage/DC signature genes averaged per cluster. Showing scaled gene expression: below mean = blue, above mean = red.
F) UMAP of *CD1C*$^+$/*CD14*$^+$ cells reclustered at high resolution from clusters within dotted line in Fig. 1C. Dashed line represents major division between clusters identified as Mono/Mac (top) and cDC2/3 (bottom)
G) PC1 and PC2 from pseudo-bulk based PCA of *CD1C*$^+$/*CD14*$^+$ cells using signature gene lists from blood cDC2, classical blood monocytes, and monocyte-derived macrophages

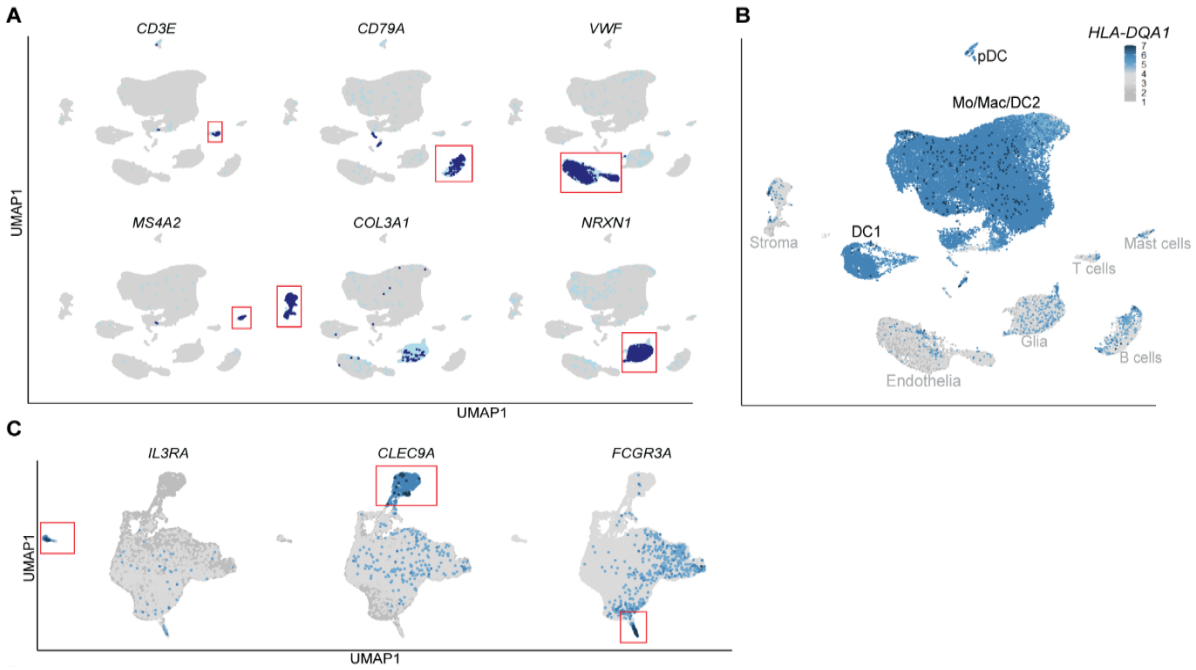

Fig S1 – Initial characterisation of cells in scRNAseq
A-B) scRNAseq data of 42,506 combined ileal and colonic LP cells, digested and enriched for HLA-DR$^+$ cells by MACS separation and FACS sorting. n = 6 colonic and 4 paired ileal CRC patients.
A) Signature genes for non-MNP cells in dataset, including T cells, B cells, endothelia, mast cells, stroma, and glia. Showing normalized gene expression.
B) Normalized *HLA-DQA1* expression
C) scRNAseq data of 28,758 computationally isolated and re-clustered MNP from combined ileal and colonic LP cells, showing normalized gene expression of signature genes for pDC, cDC1, and non-classical monocytes.

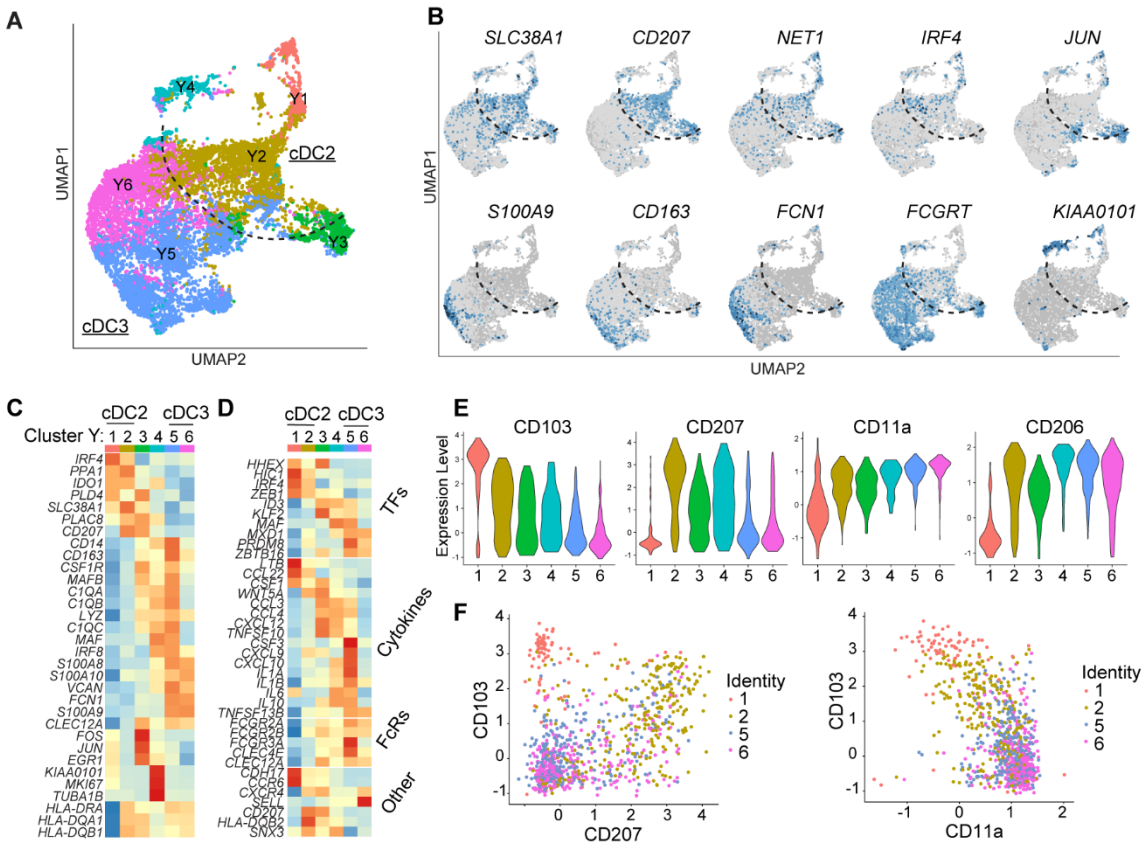

Fig 2 – Single-cell characterisation of human intestinal cDC2 and cDC3
A-D) Single-cell sequencing data of combined colon and ileum LP. Cells identified as transcriptionally cDC2-like were bioinformatically isolated and reclustered.
A) UMAP plot of isolated cDC2-like cells identified in Fig. 1. Coloured by Louvain reclustering at resolution 0.2
B) UMAP plots of cDC2 (top row) and DC3 (bottom row) normalized gene expression of signature genes
C) Curated heatmap of cDC2 and cDC3 DEG. Showing scaled gene expression: below mean = blue, above mean = red.
D) cDC2 vs. cDC3 DEG with proposed immunological functions. Showing scaled gene expression: below mean = blue, above mean = red.
E-F) Surface marker expression of DC2-like clusters analysed by CITE-seq.
E) DSB normalized surface protein expression of selected markers using CITE-seq. n = 3 CRC patients, with 3x colon LP and 1x SI LP, combined.
F) DSB normalized surface protein expression of CD103 vs. CD207 and CD103 vs. CD11a using CITE-seq. n = 3 CRC patients, with 3x colon LP and 1x SI LP, combined.

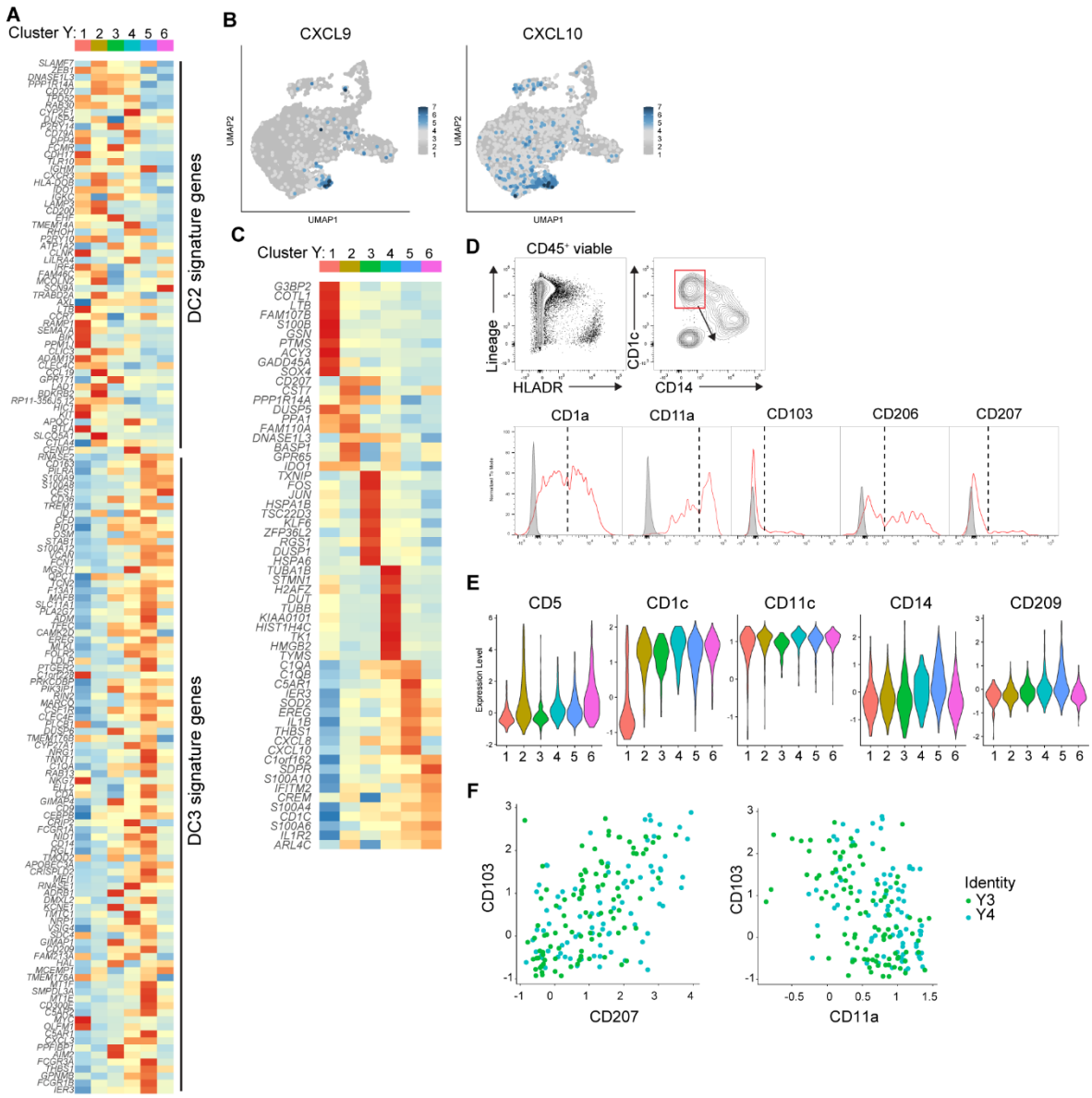

Fig S2 - Single-cell and CITEseq Characterisation of cDC2/3

A) Heatmap of genes identified as DC2 and DC3 signature genes from a peripheral blood dataset, in intestinal cDC2/3 clusters Y1-Y6. n = 6 colon and 4 ileal LP from CRC patients, combined. Showing scaled gene expression: below mean = blue, above mean = red.
B) Expression of *CXCL9* and *CXCL10* on reclustered cDC2/3 cells
C) Heatmap of top 10 DEG for cDC2/3 clusters, using scRNAseq. n = 6 colon and 4 ileal LP from CRC patients, combined. Showing scaled gene expression: below mean = blue, above mean = red.
D) 282-antibody screen (Legendscreen) showing all antibodies with bimodal expression on digested colon LP CD1c+ MNP. Best plots shown of n = 1 or 2 patients analysed per antibody.
E) Violin plots of selected DSB normalized surface marker expression on cDC2/3 clusters using CITE-seq. n = 3 colon LP and 1 ileal LP from 3 CRC patients, combined.
F) DSB normalized cite-seq expression of CD103 vs CD207 and CD103 vs CD11a, for clusters Y3 and Y4
Related to Figure 2

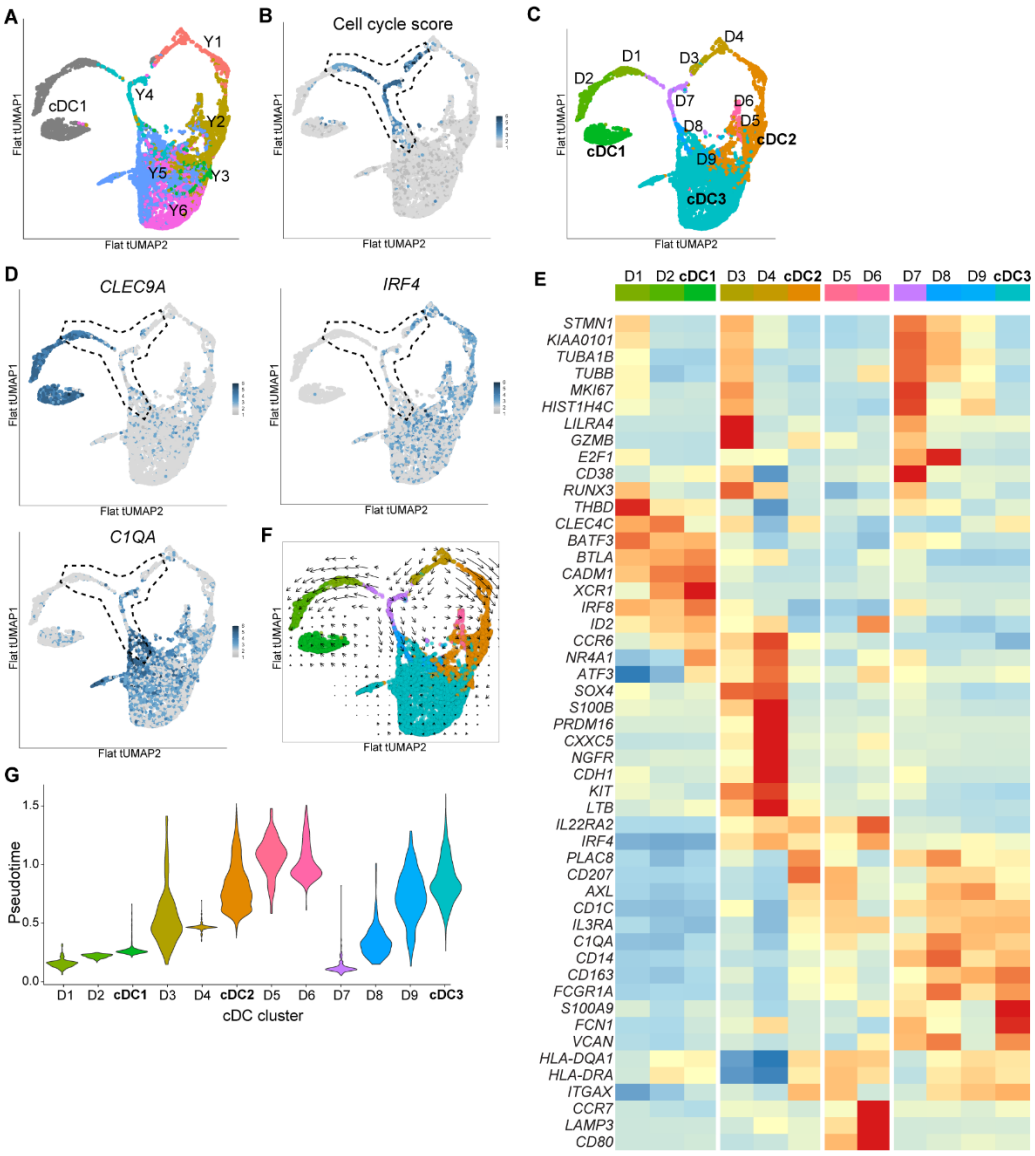

Fig 3 - cDC development in the human gut

A-D) Flattened 3D tspace UMAPs (tUMAP) (calculated with pearson on tspace PC (tPC) 1-15 and metric set to pearson) of combined cDC1, cDC2 and cDC3 scRNAseq data

A) cDC1 and Y clusters from Fig. 2, overlaid on tUMAP showing location of cDC1 (grey), cDC2 (Y2, yellow), and cDC3 (Y5, blue and Y6, pink)

B) Cell cycle module score calculated using averaged expression of cell-cycle-associated genes *KIAA0101*, *TUBA1B*, *MKI67*, *HIST1H4C*, *TUBB*, *UBE2C*, *STMN1*, and *H2AFZ*.

C) New cDC clustering with mature cDC clusters from Fig S3A compressed together. Coloured by Louvain clustering, base tPC 1-15.

D) Normalized expression of signature genes for cDC1 (*CLEC9A*), cDC2 (*IRF4*), cDC3 (*C1QA*)

E) Curated heatmap showing of genes associated with proliferation and cDC1, cDC2, or cDC3 signatures. Scaled gene expression: below mean = blue, above mean = red.

F) RNA velocities represented by arrows, calculated with Velocyto package on flattened 3D tUMAP.

G) Pseudotime score calculated as means of trajectories for each cDC cluster, starting in cluster D7, based on tSpace outputs.

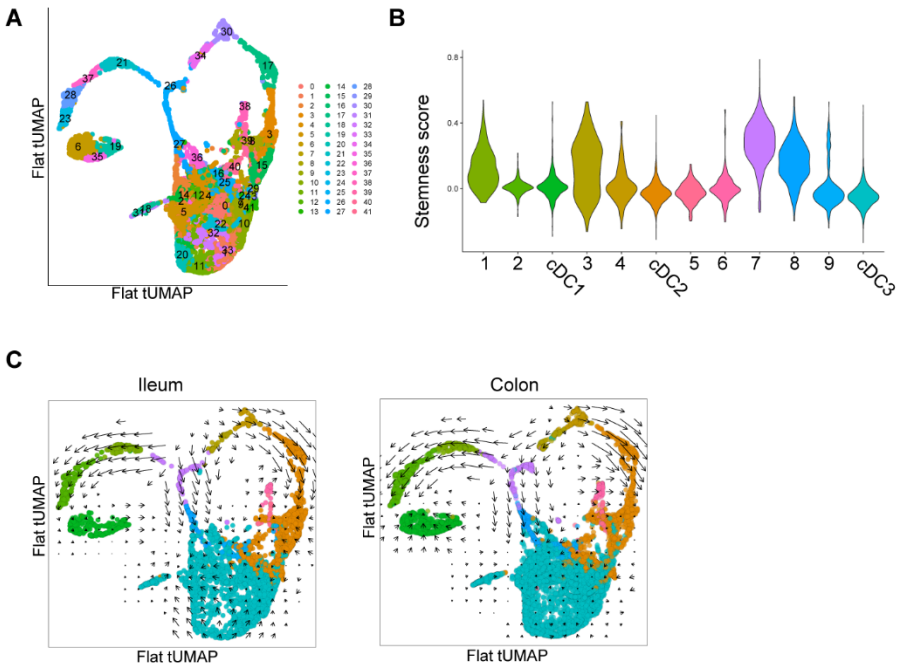

1171

Fig S3 – cDC characterisation
A) Flattened 3D tspace UMAP (tUMAP) plot of 42 clusters created from combined cDC1, cDC2, cDC3
B) 'Stemness' module score for cDC clusters composed of 20 genes (*BUB1, CND2, CDC6, CDT1, CKS2, COL18A1, CSRP2, DTYMK, HELLS, KPNA2, MCM2, MCM4, MCM5, NAP1L1, PCNA, RRM2, SHROOM3, SMO, TOP2A, TTK*) previously identified as forming a general 'stemness' signature
C) RNA velocities represented by arrows analysis for split ileum (n=4) and colon (n=6) overlayed on embeddings of 3D tUMAP.
Related to figure 3

1172

1173

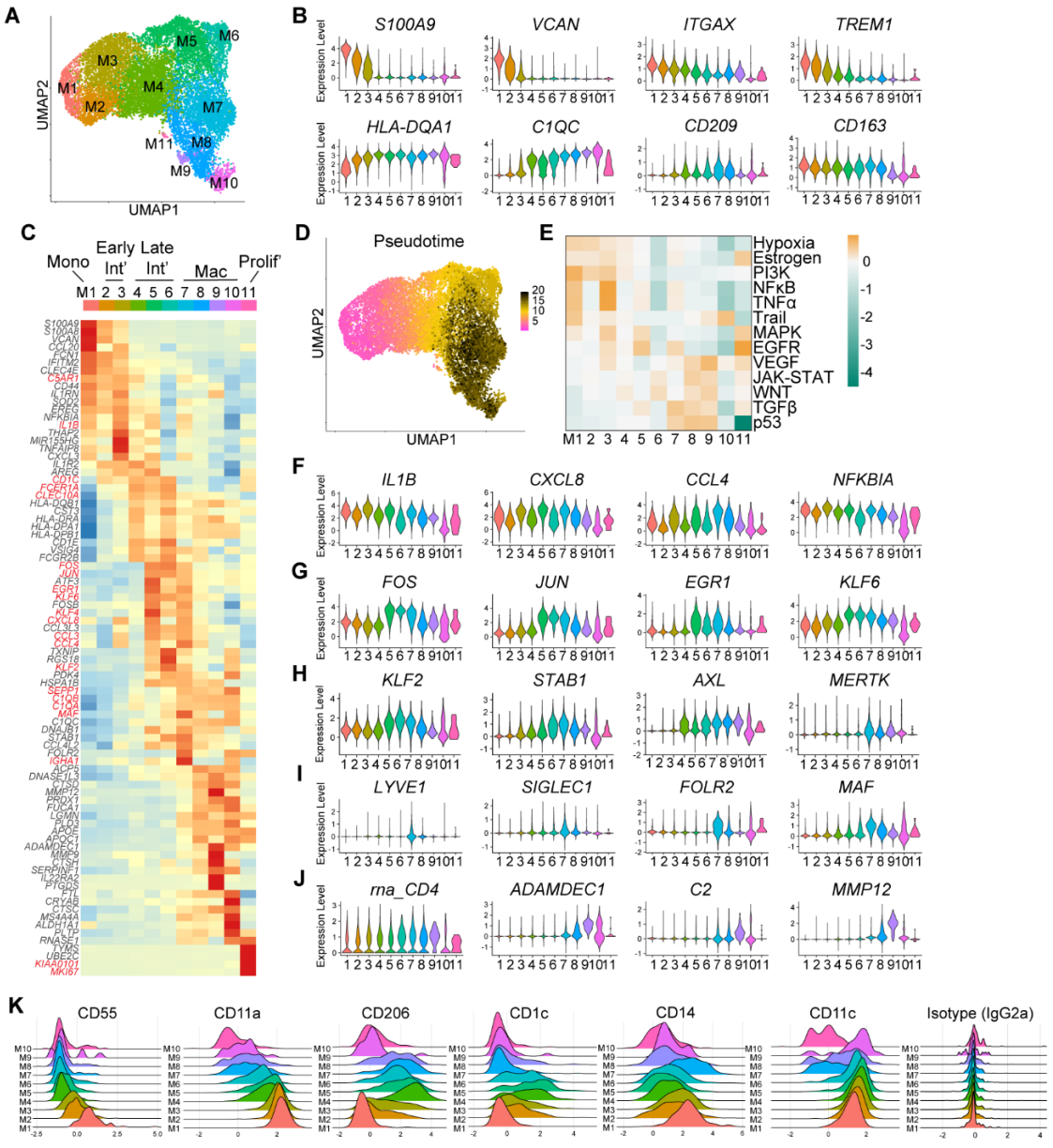

1174

Fig 4 - Characterisation of human intestinal LP monocyte/macrophage populations

A-H) tSpace analysis on computationally isolated scRNA-seq data of ileal and colonic LP cells previously identified as belonging to the monocyte-macrophage lineage.

A) tUMAP (with Seurat function) and Louvain clustering (resolution = 0.55) based tPC 1-10 of cells which were identified as Mono/Mac in Fig. 1.

B) Violin plots of normalized gene expression on Mono/Mac trajectory clusters M1-M11. DEG shown are associated with monocyte-macrophage differentiation.

C) Heatmap of select scaled gene expression by Mono/Mac trajectory clusters: below mean = blue, above mean = red.

D) Pseudotime of Mono/Mac clusters calculated from tSpace output with as means of trajectories with starting point in M1.

E) Analysis of response pathway activity in Mono/Mac trajectory clusters M1-M11 using the PROGENy package.

F-J) Violin plots of normalized gene expression by Mono/Mac trajectory clusters. DEG shown are associated with F) pro-inflammatory cytokine secretion, G) response to stimuli, H) efferocytosis, I) CD169+ perivascular macrophages, and J) self-maintaining/wound healing macrophages.

K) DSB normalized expression of surface markers on combined ileal and colonic LP Mono/Mac trajectory clusters using cite-seq, after exclusion of the the small proliferating cluster M11

1175

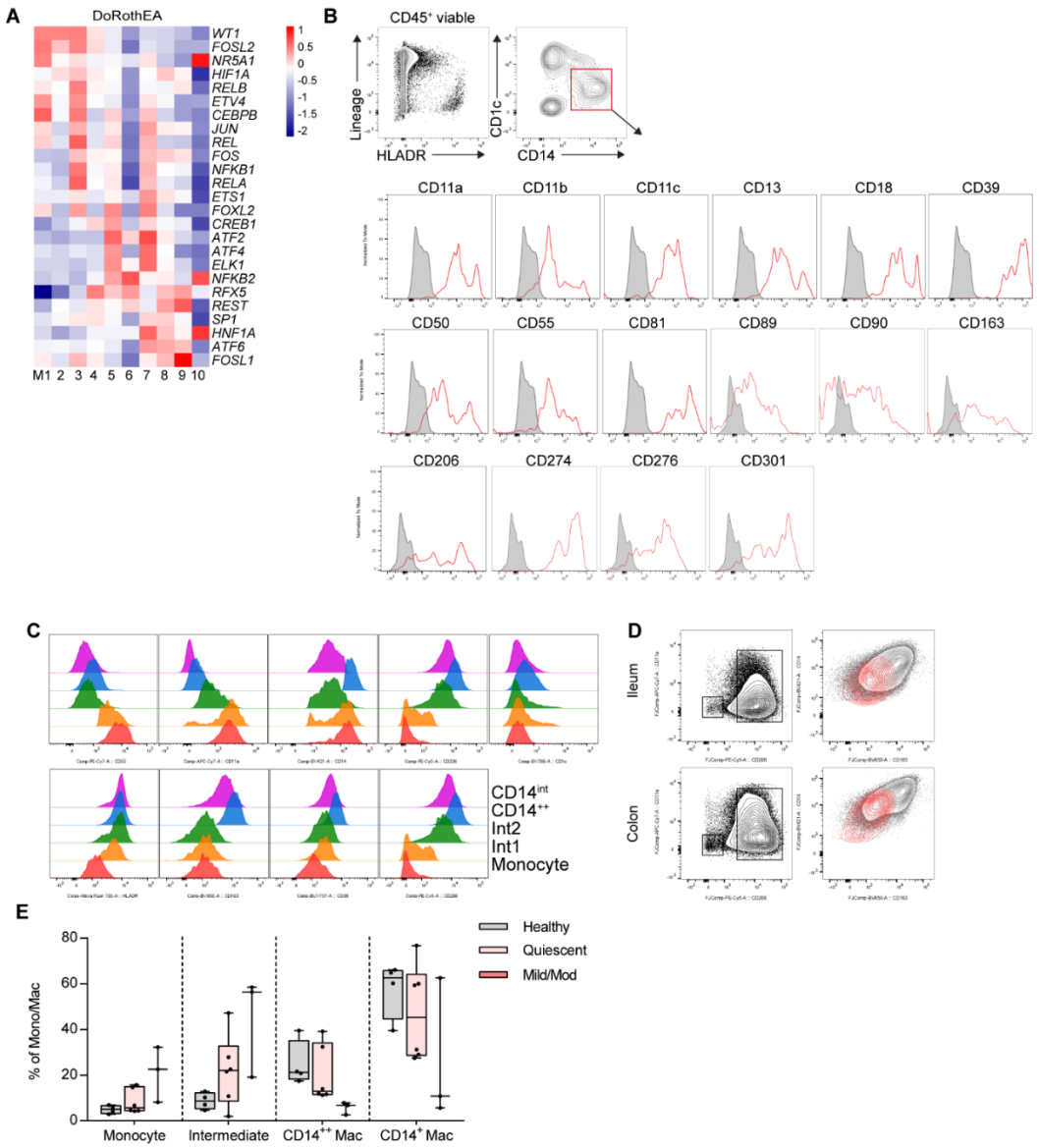

1176

Fig S4 - Monocyte - macrophage development analysis

A) Transcription factor activity inferred from target gene expression in Mono/Mac trajectory clusters M1-M10, using the DoRothEA package.

B) Representative staining of all antibodies with bimodal expression on CD14+ MNP in 361-antibody screen (Legendscreen). Samples taken from digested colonic LP tissue from CRC patients. n= 1-2 patients tested per antibody. Gated on viable CD45+ HLADR+ lin- cells. Grey line = FMO, red line= specific antibody stain.

C) Representative surface marker expression of colonic LP Mono/Mac subsets using flow cytometry. Gated on viable CD45+ HLADR+ lin- cells.

D) Gating strategy to identify CD206- CD11a- macrophages within the CD14+ CD55+ gate. Samples concatenated from digested ileal and colonic LP tissue taken from 10 CRC patients.

E) Mono/Mac subset frequencies in ileal IBD and non-IBD biopsies. Samples were taken during IBD surveillance endoscopy and tissue inflammation was scored at the time of the procedure by the clinican. n = 5-13 samples, some samples with different inflammatory scores were taken from the same patient

Related to figure 4

1177

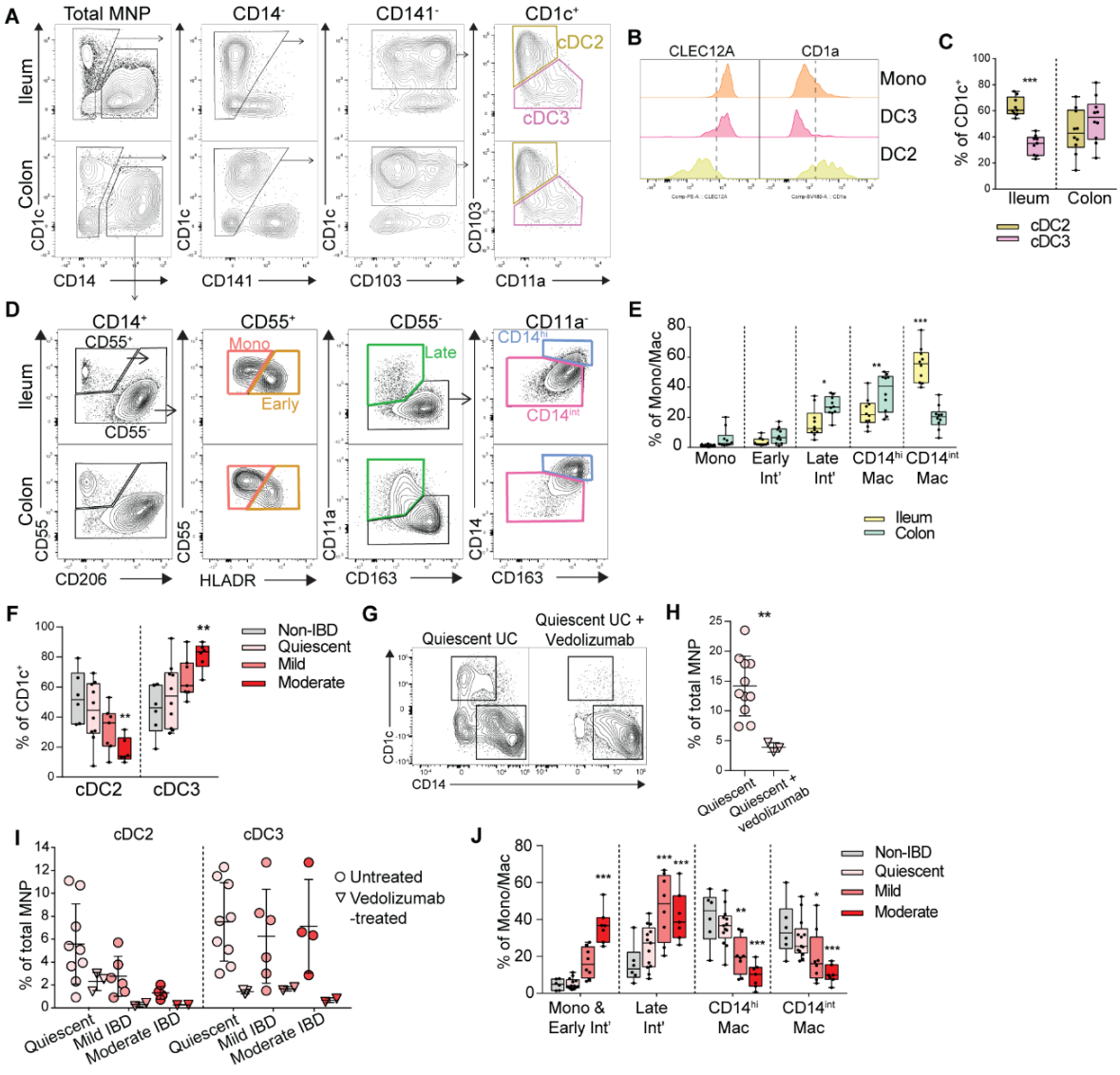

1178

Fig 5 - Flow cytometry analysis of MNP subsets

A-E) Flow cytometry analysis of digested tissue taken from unaffected colonic and ileal LP of colorectal cancer patients. n = 10 paired ileal and colonic samples.

A) Gating strategy distinguishing CD1c+ CD103+ CD11a- cDC2 from CD1c+ CD103+ CD11a+ cDC3 in ileum and colon using either CD103 vs. CD207 or CD103 vs. CD11a, gating on total viable CD45+ MNP

B) CD11a- CD103+ cDC2 and CD11a+ CD103- cDC3 frequency of total CD14- CD1c+ MNP in ileal and colonic LP. n = 9 CRC patients

C) Representative histograms of CLEC12A and CD1a expression on CD14+ CD55+ CD206- monocytes, CD1c+ CD103+ CD11a- cDC2, and CD1c+ CD103+ CD11a+ cDC3 from colon resection

D) Gating strategy to identify monocytes, monocyte-derived early and late intermediates, and two subsets of macrophage

E) Analysis of monocytes and monocyte-derived MNP subsets as a proportion of total CD14+ cells in colonic and ileal LP

F-J) Flow cytometry analysis of digested tissue taken from colonic biopsies. Extent of IBD inflammation was scored at the time of biopsy by the clinician as quiescent, mild, or moderate. n = 5-13 samples, some samples with different inflammatory scores were taken from the same patient.

F) $CD11a^{-}$ $CD103^{+}$ cDC2 and $CD11a^{+}$ $CD103^{-}$ cDC3, as proportion of $CD14^{-}$ $CD1c^{+}$ MNP, from colonic biopsies. n = 6-10 biopsies from sites of quiescent, mild, or moderate IBD inflammation, or from non-IBD controls. Statistical significance was determined using 2-way ANOVA with Dunnett's multiple comparisons, **p<0.01

G) Representative flow cytometry plots of CD1c vs CD14 stains of UC patient colon LP MNP, with or without vedolizumab treatment

H) $CD1c^{+}$ MNP as proportion of total MNP from IBD biopsies, with or without vedolizumab treatment. n = 3-11 biopsies from sites of quiescent IBD inflammation. Statistical significance was determined using Student's T test, **p<0.01

I) $CD11a^{-}$ $CD103^{+}$ cDC2 and $CD11a^{+}$ $CD103^{-}$ cDC3 MNP, as proportion of total MNP from IBD biopsies, with or without vedolizumab treatment. n = 2-9 biopsies from sites of quiescent, mild, or moderate IBD inflammation

J) Mono/Mac subsets as proportion of $CD14^{+}$ $CD1c^{lo}$ MNP, from colonic biopsies. n = 6-14 biopsies from sites of quiescent, mild, or moderate IBD inflammation, or from non-IBD controls. Some points represent single patients with samples taken from multiple sites with different levels of inflammation. Statistical significance was determined using 2-way ANOVA with Dunnett's multiple comparisons, *p<0.05, **p<0.01 ***p<0.001

1179

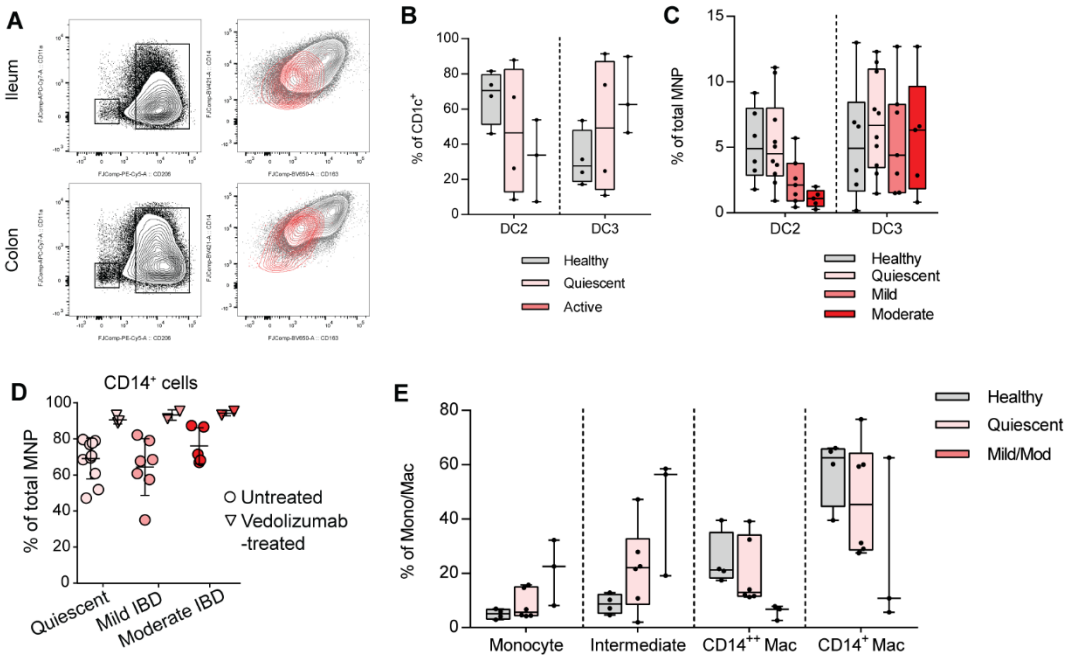

1180

Fig S5 - Flow cytometry analysis of MNP subsets

A) Flow cytometry analysis of CD206$^-$ macrophages from 10 concatenated ileal and colonic resection samples. Gated on CD14$^+$ CD55$^-$ MNP

B) CD11a$^-$ CD103$^+$ cDC2 and CD11a$^+$ CD103$^-$ cDC3, as proportion of CD1c$^+$ MNP, in ileal biopsies. n = 3 to 4 patients from sites of quiescent, mild/moderate IBD inflammation, or from non-IBD controls. Some points represent single patients with samples taken from multiple sites with different levels of inflammation.

C) CD11a$^-$ CD103$^+$ cDC2 and CD11a$^+$ CD103$^-$ cDC3, as proportion of HLADR$^+$ lineage$^-$ MNP, in colonic biopsies. n = 5 to 10 patients, some points represent single patients with samples taken from multiple sites with different levels of inflammation. Lines represent range of data, boxes represent 25th to 75th percentile intersected by median.

D) CD14$^+$ cells (monocytes/macrophages) as proportion of total HLADR$^+$ lineage$^-$ MNP from IBD biopsies, with or without vedolizumab treatment. Biopsies taken from 5 different sites from 3 vedolizumab-treated patients. Lines represent median ± SD.

E) Mono/Mac subsets as proportion of CD14$^+$ CD1c^{lo} MNP, from ileal biopsies. n = 3-6 biopsies from sites of quiescent, mild/moderate IBD inflammation, or from non-IBD controls. Some points represent single patients with samples taken from multiple sites with different levels of inflammation.

Related to figure 5

1181

1182

1183